J. Nonlinear Sci. Vol. 12: pp. 241–281 (2002)
DOI: 10.1007/s00332-002-0493-1

Journal of
Nonlinear
Science

Tendril Perversion in Intrinsically Curved Rods

T. McMillen[1] and A. Goriely[1,2]
[1]Program in Applied Mathematics and [2]Department of Mathematics,
University of Arizona, Building #89, Tucson, AZ 85721, USA

Received September 19, 2001; accepted January 25, 2002
Online publication April 30, 2002
Communicated by P. Holmes

Summary. A straight elastic rod with intrinsic curvature under varying tension can undergo an instability and bifurcate to a filament made out of two helices with opposite handedness. This inversion of handedness, known as perversion, appears in a wide range of biological and physical systems and is investigated here within the framework of thin elastic rods described by the static Kirchhoff equations. In this context, a perversion is represented by a heteroclinic orbit joining asymptotically two fixed points representing helices with opposite torsion. A center manifold reduction and a normal form transformation for a triple zero eigenvalue reduce the dynamics to a third-order reversible dynamical system. The analysis of this reduced system reveals that the heteroclinic connection representing the physical solution results from the collapse of pairs of symmetric homoclinic orbits. Results of the normal form calculation are compared with numerical solutions obtained by continuation methods. The possibility of self-contact and the elastic characteristics of the perverted rod are also studied.

Key words. elastic rods, intrinsic curvature, differential growth, heteroclinic orbits, center manifolds, normal forms, self-contact, helical springs

1. Introduction

In nature, long thin filamentary structures are observed from the microscopic chains of molecules to the macroscopic braided magnetic flux tubes in solar flares. The central problem in the study of filaments is to understand the possible changes of configurations and the dynamics involved in the changes. Filaments at all sizes seem to follow universal configuration changes triggered by generic instabilities. Consider, for instance, the

Correspondence to: A. Goriely, goriely@math-arizona.edu

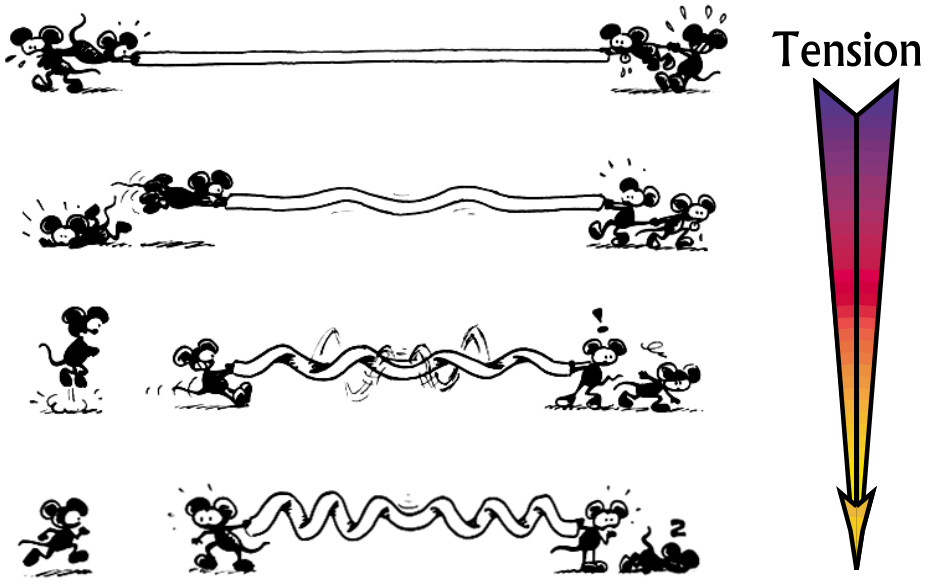

Fig. 1. A cartoon of the *curvature-to-writhe* instability; as the tension is decreased, the instability sets in and two helices with opposite handedness are created: *a perversion*.

coiling of strings, ropes, or telephone cords. If you take a piece of rubber tubing, hold it between your fingers, and twist its ends, the filament will soon coil on itself. This is an example of a *writhing instability* where a local change in twist eventually results in a global reconfiguration of the filament. In this case we have a *twist-to-writhe* conversion. The word *writhe* refers to global deformation of a filamentary structure. This type of instability has received considerable interest and is known to be important in processes such as coiling and super-coiling of DNA structures [1], [2], [3] and morphogenesis in bacterial filaments [4], [5], [6].

Another type of writhing instability is the *curvature-to-writhe* instability where changes of curvature trigger global shape reconfigurations [7]. This instability can also be observed in telephone cords. If one completely untwists the helical structure of the cord and pulls the ends, a straight cord can be obtained. Now, if one slowly releases the ends, the filament suddenly changes shape to a structure composed of two helical structures with *opposite handedness* and linked by a small inversion (see Fig. 1). We refer to this structure as a *perversion*. The German mathematician J. B. Listing [8], [9] refers to an inversion of chirality as *perversion* as used by D'Arcy Thompson to characterize seashells: "the one is a mirror-image of the other; and the passing from one to the other through the plane of symmetry (which has no 'handedness') is an operation which Listing called *perversion*" [10, p. 820]. Maxwell, in his 1873 treatise on electromagnetism, also uses the word perversion: "They are geometrically alike in all respects, except that one is the perversion of the other, like its image in a looking glass" [11]. The usage of the word *perversum* actually originated in the description of rare left-handed specimens of

Fig. 2. An actual perversion in a telephone cord.

seashells in a species of overwhelming right-handed individuals (for instance, there are only six known left-handed specimens out of the million known *Cerion*, a West Indian land snail [12], [13]).

A qualitative explanation of the creation of helices with opposite handedness (see Fig. 2) can readily be given. Consider a filament with given nonvanishing intrinsic curvature, that is, the unstressed configuration is coiled on itself (a multicovered ring, if ones disregards self-contact). Now, take this filament and completely untwist it and straighten it out. By applying sufficient tension (and proper end moments), one can completely straighten out the filament. Note that the total twist of the straight filament is zero. Now, as one reduces the tension, there is a critical value of the tension below which the straight filament becomes unstable. The *optimal* solution (the solution with lowest energy) is a helix whose torsion and curvature are functions of the tension. However, in order to create a helix, one of the ends must rotate. As we do not allow the ends to rotate, this solution cannot be obtained. Nevertheless, another solution with zero twist can be obtained by smoothly pasting two optimal helices together with a small inversion. This is the perversion solution. It can be obtained by reducing the tension of an intrinsically curved twistless straight filament whose total twist is fixed. One of the most fascinating natural manifestations of perversion can be found in the growth of some climbing plants. Among the many different mechanisms climbing plants use to climb and grow along supports, the so-called tendril-bearers constitute an important class (e.g., the grape-vine, the hop, the bean, the melon). In the first stage of their development, tendrils are tender, soft, curly, and flexible organs originating from the stem. As they grow, the tendrils *circumnutate* [15], [16]. That is, the tip of the tendril describes large loops in space by completely rotating on itself until it touches a support, such as a trellis, a pole or a branch. If the circumnutation does not result in a contact, the tendril eventually dries and falls off the stem. The tendrils which are in contact with a support enter another phase of their development, and their tissues develop in such a way that they start to curl and tighten up, eventually becoming woody, robust, and tough. This curling provides the plant with an elastic springlike connection to the support that enables it to resist high winds and loads. Since neither the stem nor the support can rotate, the total twist in the tendril cannot change. Thus the conditions are ripe for obtaining a perversion, and as the tendril curls on itself, the coils of the helix are reversed at some point so that the tendril goes from a left-handed helix to a right-handed one, the two being separated by a small inversion, the perversion (see Fig. 3).

The phenomenon of perversion in climbing plants has a long, interesting scientific history. Inversion of helicity in tendrils already appears in the illustration (see Fig. 4) of Linnaei in *Philosophia Botanica* [17]. However, according to de Candolle [18], [19], the first record of a scientific observation of perversion goes back to a letter of the French scientist Ampère to the French Academy of Sciences. From then on, almost all major botanists in the nineteenth century, such as Dutrochet in 1844 [20], von Mohl in 1852 [21], and Léon in 1858 [22], [23] describe the perversion found in tendrils.

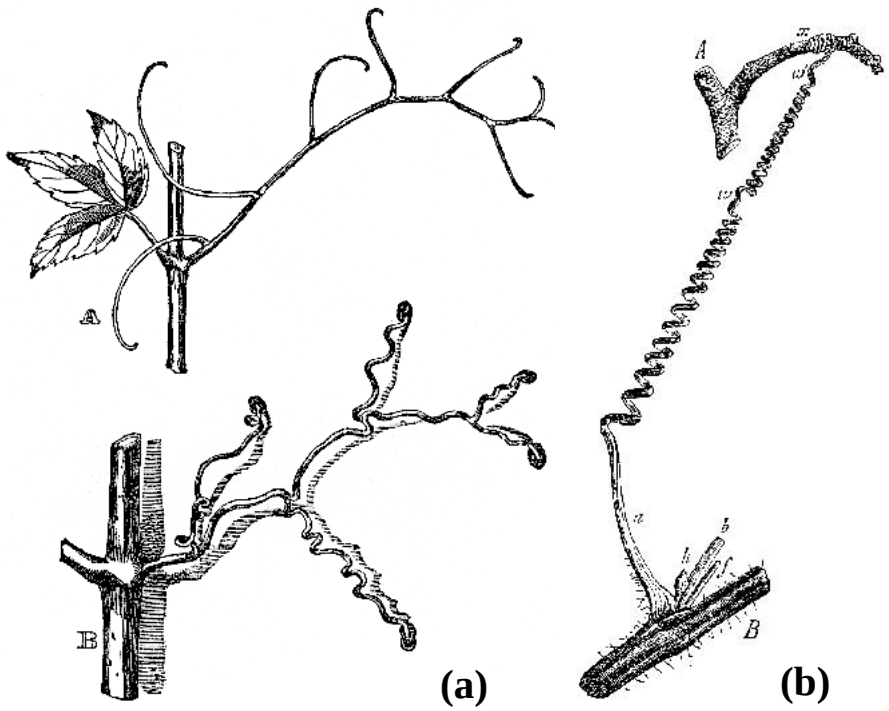

Fig. 3. (a) Growth of climbing plants (tendril bearers) as drawn by Darwin [14]. In the first stage (A), the tendrils are *circumnutating* until they find an attachment. In the second stage (B), the tendrils are attached and perversion sets in. (b) Another example of tendril perversion in Bryonia dioica. Illustration from Sachs's *Text-book of Botany* (1875).

It is Charles Darwin, inspired by related studies by his friend, the American botanist, Asa Gray [24], who gave the first complete and truly scientific analysis of the growth of climbing plants in his delightful little book *The Movements and Habits of Climbing Plants* [14] based on an essay presented at the Linnean Society in 1865. In there, among many other observations (such as the spiral growth of stems and the phenomenon of circumnutation), he devotes a whole chapter on the problem of tendril growth and gives the first qualitative explanation for the inversion: "when a tendril has caught a support and is spirally contracted, there are always as many turns in one direction as in the other; so that the twisting of the axis in the one direction is exactly compensated by the twisting in the opposite direction. . . . I cannot resist giving one other illustration, though superfluous: When a haberdasher winds up ribbon for a customer, he does not wind it into a single coil; for, if he did, the ribbon would twist itself as many times as there were coils; but he winds it into a figure of eight on his thumb and little finger, so that he alternately takes turns in opposite directions, and thus the ribbon is not twisted. So it is with tendrils, with this sole difference, that they take several consecutive turns in one direction and then the same number in an opposite direction; but in both cases the self-twisting is avoided" (see Fig. 5).

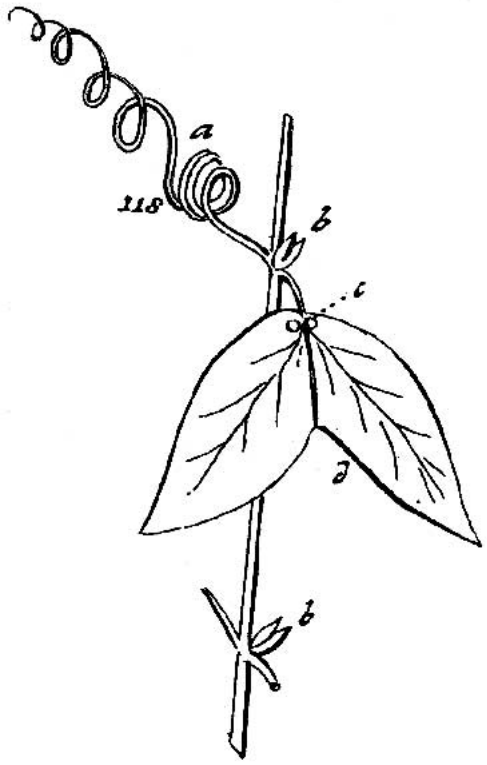

Fig. 4. Climbing plants (right-handed) with tendrils (with perversion) as drawn by Linnaei in *Philosophia Botanica* [17].

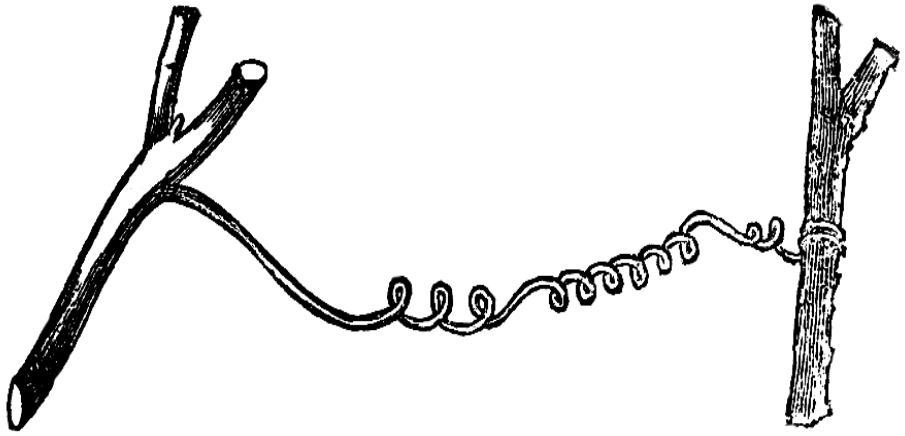

Fig. 5. Tendril perversion as drawn by Darwin [14].

Another striking occurrence of perversion can be found in the structure of human umbilical cords. Umbilical cords are generally made out of two arteries and one vein embedded in a compact gel-like structure known as the Wharton jelly [25]. The arteries are longer than the vein, which is itself longer than the jelly, and therefore the cord forms a triple helix. The handedness of this helix was already described in 1521 by Berengarius [26] and has fascinated medical doctors and scientists since then [27]. The umbilical cord is on average 50–60cm long with up to 40 helical turns, and helicity can be observed as early as 42 days' gestation [28]. Umbilical cords can be either left-handed, right-handed, straight, or with mixed helicity. Strangely enough, the ratio of left-handed to right-handed cords is about 7 to 1, the usually accepted ratio of right-handed to left-handed adults. However, there does not seem to be any statistical correlation between the handedness of the cord and the hand preference as an adult [29]. According to different statistical studies, inversion from left-handed to right-handed structure in umbilical cords varies from 2% to 26% of all cases [27], [30]. This discrepancy comes from the fact that most studies have not focussed on perverted umbilical cords and have classified some of them as predominantly right- or left-handed cords. To date, there is no model for the growth of umbilical cords that would explain the difference or handedness, its inversion or even the occurrence of helicity. Both genetic and mechanical factors seem important as the correlation between umbilical cord helicity in monozygotic twins [26] and experiments on the effect of tension on fetal activity in laboratory rats indicate [31], [32]. In light of the present work, we propose that the onset of umbilical perversion is the result of biased differential growth of the cord with external constraints such as tension and blockage of twist.

Inversion of helicity appears also in the microscopic world. The flagella of some bacteria such as *Salmonella* or *E. coli* have helical shapes. These flagella, about 4μm long, are composed of a few protofilaments made out of a single protein. Depending on the respective position of the different protofilaments, the flagella can be, in their unstressed configuration, either right-handed or left-handed [33], [34], [35], [36]. They are attached to the cell-body through a molecular rotary motor [37] and are observed to flip from a left- to a right-handed helix when the running motion is interrupted by a tumble motion [38], [39]. This inversion of helicity plays a crucial role in the ability of the bacterium to change direction of motion and is performed by propagating a right-handed helix onto a left-handed helix, henceforth creating a perversion [40]. Perversion can also be observed in a variety of other microscopic biological systems: in the shape of certain bacteria such as spirochetes [41], in some mutant forms of *B. subtilis* [42], in the microscopic structure of cotton fibers [43], or in the shape of miniature (1 to 2 mm long) seashells [44]. Finally, in the textile industry, there is a specific method used to roughen yarns and based on the creation of inversion along the fibers, known as the false-twist technique [45].

Perversion in tendrils was first modeled by Keller [46], who derived the equations governing the shape of tendrils based on the assumption that the shape is a minimizer of the energy of the system (composed of the elastic energy given by the strains and the potential energy of the force applied). Recently, Goriely and Tabor [7] identified the role of intrinsic curvature and studied the formation of a perversion as a dynamical solution of the Kirchhoff equations. They found the critical value of the tension that gives rise to a perversion for both finite and infinite filaments, together with the time-exponents associated to these solutions (in the inertial case). Here, we study the onset of

perversion in elastic rods with intrinsic curvature by using the static Kirchhoff equations for thin elastic rods with linear constitutive relationships. We study the problem from a dynamical system perspective [47], [48], [49] and show that perversion can be represented in this setting by heteroclinic orbits. We use the first integrals of the problem to identify the asymptotic helices that perversion solutions connect and compute the mechanical properties of the perversion. This approach and the numerical analysis performed in the last section generalize and complement the results obtained in [7], which was mostly a linear analysis of the solution and its dynamics. The role of intrinsic curvature in the stability of elastic filaments within the context of the Kirchhoff equations has also been considered for closed twisted ring solutions [50], helical filaments [51], twisted straight filaments under tension [52], and in the shape of DNA molecules [53].

2. The Kirchhoff Model

We use the Kirchhoff model of elastic rods to describe the statics of rods with intrinsic curvature. In the Kirchhoff model, an elastic rod is represented by a space curve with given physical properties. The space curve represents the central axis, the properties of the rod are shape (how it is oriented in space), stiffness (elastic properties of a particular rod), twist (how adjacent cross-sections are oriented along the length of the rod), and spin (how a cross-section rotates in time). The external stresses, forces, and moments acting on the rod are averaged over cross-sections of the filament.

2.1. Kinematics

A *ribbon* is defined as a pair given by a *space curve*, $\mathbf{x}(s,t)$ together with a unit *basis vector* $\mathbf{d}_1(s,t)$ lying in a plane normal to the curve. Here, s is the arclength and t is time, i.e., for each t, $\mathbf{x}(s,t)$ and $\mathbf{d}_1(s,t)$ are C^3 maps from an interval of $\mathbb{R}$ (possibly infinite) into $\mathbb{R}^3$. The kinematics of ribbons is described in terms of a *director basis*,

$$(\mathbf{d}_1, \mathbf{d}_2, \mathbf{d}_3) = (\mathbf{d}_1(s,t), \mathbf{d}_2(s,t), \mathbf{d}_3(s,t)), \tag{1}$$

where the basis vector $\mathbf{d}_3(s,t)$ is the *tangent vector* to the curve:

$$\mathbf{d}_3 \equiv \mathbf{x}', \tag{2}$$

and $(\cdot)' \equiv \partial(\cdot)/\partial s$, $\dot{(\cdot)} \equiv \partial(\cdot)/\partial t$. The introduction of ribbons rather than space curves allows one to attach to a space curve material properties such as twist, intrinsic curvature, or bending stiffness (see next section). The vector $\mathbf{d}_1$ will be chosen so as to follow that particular material property. For instance, in the case of rods with elliptical cross-sections, one can choose the vector $\mathbf{d_1}$ to follow the direction of the major or minor axis (see Fig. 6). The vector $\mathbf{d}_2 = \mathbf{d}_3 \times \mathbf{d}_1$ is then chosen so that $(\mathbf{d}_1, \mathbf{d}_2, \mathbf{d}_3)$ is a right-handed orthonormal basis. We can measure the twist and spin in the filament by measuring how much the basis twists or spins as s or t varies. The requirement that the basis remains orthonormal in space and time implies the existence of a *twist vector* $\boldsymbol{\kappa}$ and a *spin vector* $\boldsymbol{\omega}$ satisfying

$$\mathbf{d}_i' = \boldsymbol{\kappa} \times \mathbf{d}_i, \qquad i = 1,2,3, \tag{3}$$

$$\dot{\mathbf{d}}_i = \boldsymbol{\omega} \times \mathbf{d}_i, \qquad i = 1,2,3. \tag{4}$$

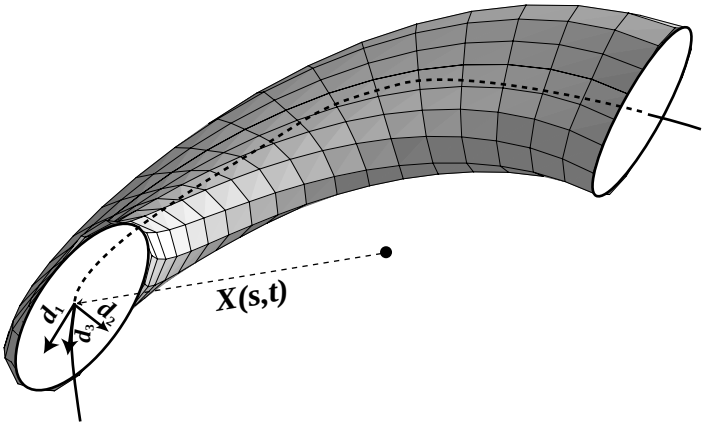

Fig. 6. A filament with noncircular cross-section, showing the basis vectors $\mathbf{d}_1$ and $\mathbf{d}_2$. The vector $\mathbf{d}_3$ is tangent to the central axis curve $\mathbf{x}(s, t)$.

The director basis ($\mathbf{d}_1, \mathbf{d}_2, \mathbf{d}_3$) can be related to the Frenet basis ($\mathbf{n}$, $\mathbf{b}$, $\mathbf{t}$) (normal, binormal, and tangent vectors) by introducing on each cross-section an angle ζ between the normal vector and $\mathbf{d}_1$. Then, the Frenet curvature κ and torsion τ defined through the Frenet equations

$$\mathbf{t} = \mathbf{x}', \qquad \mathbf{t}' = \kappa\mathbf{n}, \qquad \mathbf{b} = \mathbf{t} \times \mathbf{n}, \qquad \mathbf{b}' = -\tau\mathbf{n}, \tag{5}$$

are related to the components of the twist vector by

$$\boldsymbol{\kappa} = (\kappa \sin(\zeta), \kappa \cos(\zeta), \tau + \zeta'). \tag{6}$$

Here, κ_1 and κ_2 are the components of curvature, while κ_3, called the *twist density*, contains information on both the torsion of the curve and the twist of the filament. We adopt the standard convention that the curvature $\kappa \geq 0$ and the torsion $\tau \in \mathbb{R}$. The derivative ζ' measures the change in the angle between $\mathbf{d}_1$ and the normal to the curve; this is the *twist*. The twist thus measures how consecutive cross-sections rotate along the filament. The twist is distinguished from the *total twist* of the filament defined as $\int \kappa_3 ds$, where the integral is taken over the length of the filament. The total twist measures the total number of turns a basis vector makes along the full length of the filament, relative to a fixed vector. Thus, the total twist is a global property of a filament depending on both torsion and twist, whereas the twist is a local property defined at each point s along the filament.

2.2. Dynamics

We assume that the filament is inextensible, unshearable, and has constant cross-section. The vector $\mathbf{d}_1$ is chosen to lie along one of the principal axes of inertia of the filament's cross-section. The Kirchhoff model relates the force and moment, called $\mathbf{F}$ and $\mathbf{M}$, respectively, acting across cross-sections of the filament to the director basis. The balance

of linear and angular momenta across each cross-section leads to the Kirchhoff equations [54], [55],

$$\mathbf{F}' = \xi A \ddot{\mathbf{x}}, \tag{7}$$

$$\mathbf{M}' + \mathbf{d}_3 \times \mathbf{F} = \xi (I_2 \mathbf{d}_1 \times \ddot{\mathbf{d}}_1 + I_1 \mathbf{d}_2 \times \ddot{\mathbf{d}}_2), \tag{8}$$

where ξ is the (constant) mass per unit volume of the rod and A is the cross-sectional area; the quantities I_1 and I_2 are the principal moments of inertia of the cross-section.

The *unstressed state* is the stationary shape of a filament with no external constraints. This state can be defined by its *intrinsic curvature*, which we call

$$\boldsymbol{\kappa}^{(u)} = \kappa_1^{(u)} \mathbf{d}_1 + \kappa_2^{(u)} \mathbf{d}_2 + \kappa_2^{(u)} \mathbf{d}_2. \tag{9}$$

The Kirchhoff equations are then closed by the constitutive relation of linear elasticity theory:

$$\mathbf{M} = E I_1 (\kappa_1 - \kappa_1^{(u)}) \mathbf{d}_1 + E I_2 (\kappa_2 - \kappa_2^{(u)}) \mathbf{d}_2 + \mu J (\kappa_3 - \kappa_3^{(u)}) \mathbf{d}_3, \tag{10}$$

where E is Young's modulus, μ is the shear modulus, and J is a geometric factor depending on the cross-sectional shape [56]. The elastic energy density of the filament is given by

$$\mathcal{E} = \mathbf{M} \cdot (\boldsymbol{\kappa} - \boldsymbol{\kappa}^{(u)}), \tag{11}$$

so that the state of lowest elastic energy is given by $\boldsymbol{\kappa} = \boldsymbol{\kappa}^{(u)}$, the *unstressed* state.

2.3. Statics and Rescaling

In the static case, all time derivatives in (7–8) are set to zero, and the system becomes

$$\mathbf{F}' = 0, \tag{12}$$

$$\mathbf{M}' + \mathbf{d}_3 \times \mathbf{F} = 0. \tag{13}$$

We rescale the system by choosing combinations of the length $[L]$, time $[T]$, and mass $[M]$ units in the following way:

$$[M] = \xi \sqrt{A I_1}, \qquad \frac{[M][L]^3}{[T]^2} = E I_1, \tag{14}$$

which amounts to making the substitution

$$\mathbf{M} \to \frac{E I_1}{L} \mathbf{M}, \qquad \mathbf{F} \to \frac{E I_1}{L^2} \mathbf{F}, \tag{15}$$

$$s \to L s, \qquad \boldsymbol{\kappa}, \boldsymbol{\kappa}^{(u)} \to L^{-1} \boldsymbol{\kappa}, \boldsymbol{\kappa}^{(u)}. \tag{16}$$

In the static case, the L remains arbitrary. This contrasts with the dynamic case, in which we must choose $L = \sqrt{A/I_1}$ in order to nondimensionalize the equations (7–8). This degree of freedom remains in the static case because the force $\mathbf{F}$ contains a time scale

which remains arbitrary in the static case. Then, the static Kirchhoff equations reduce to the scaled form

$$\mathbf{F}' = 0, \tag{17}$$

$$\mathbf{M}' + \mathbf{d}_3 \times \mathbf{F} = 0, \tag{18}$$

$$\mathbf{M} = (\kappa_1 - \kappa_1^{(u)})\mathbf{d}_1 + \Lambda(\kappa_2 - \kappa_2^{(u)})\mathbf{d}_2 + \Gamma(\kappa_3 - \kappa_3^{(u)})\mathbf{d}_3, \tag{19}$$

where $\Lambda = I_2/I_1$ is the ratio of moments of inertia and $\Gamma = \mu J/EI_1$ is the ratio of torsional stiffness to the bending stiffness in the direction $\mathbf{d}_1$. The asymmetry in the filament is measured by Λ. The choice of axis along which $\mathbf{d}_1$ lies determines whether Λ is larger or smaller than unity. If we choose $\mathbf{d}_1$ to lie in the direction of the largest bending stiffness, that is $I_1 \geq I_2$, we have $\Lambda \leq 1$, whereas, in the case $I_1 \leq I_2$, we have $\Lambda \geq 1$. In the case of a circular cross-section, $I_1 = I_2$, and

$$\Lambda = 1, \qquad \Gamma = (1+\sigma)^{-1} \in [2/3, 1], \tag{20}$$

where σ is Poisson's ratio. Values of Γ near 1 correspond to incompressible material such as steel, while values near 2/3 correspond to hyperelastic material such as rubber.

The equations (2), (3), and (17–19) form a closed system. This system decouples, so that one may solve (17–19), then (3), then (2), separately. Thus, we obtain a complete description of the filament by solving (17–19).

The quantities in the scaled system (17–19) still have a dimension. From (19), we see that the scaled moment $\mathbf{M}$ has the dimension of an inverse length, and that the scaled force $\mathbf{F}$ has the dimension of the inverse of a squared length; hence every variable involved is a length to a power. However, the system cannot be further simplified by choosing the length unit $[L]$, because the remaining constants Λ and Γ are already dimensionless. Nevertheless, it is still possible to choose a convenient length scale for a given problem. For example, if we consider a finite rod, a natural choice for L is the length of the rod. Another natural length scale, in the case of a rod which is a ring in its unstressed state, is the radius of the ring. Yet another length scale which is convenient for certain cases is the radius of the rod if the rod has a circular cross-section.

The fact that the length unit $[L]$ is undetermined has yet another implication. Considering the static system (17–19), we see that every known solution actually determines a one-parameter family of solutions. More precisely, if $\{\mathbf{F}(s), \mathbf{M}(s), \boldsymbol{\kappa}(s)\}$ is a solution of the system, then $\{\lambda^{-2}\mathbf{F}(\lambda s), \lambda^{-1}\mathbf{M}(\lambda s), \lambda^{-1}\boldsymbol{\kappa}(\lambda s)\}$ is another solution of the system for every real nonvanishing λ. That is, the system is *scale-invariant*. Furthermore, if such a transformation is performed on the solution together with a rescaling of the length unit $[L]$ by a factor λ^{-1}, the solution remains unchanged, although the rod thickness is modified by a factor λ^{-1}. Hence, the statics of a filament, in the Kirchhoff model, is independent of the rod thickness.

2.4. Intrinsic Curvature

Intrinsic curvature describes the property of materials which in their unstressed states have locally a nonvanishing curvature. In terms of the unstressed curvature vector, we

consider materials which (*i*) only exhibit intrinsic curvature (no intrinsic twist or torsion), (*ii*) in their unstressed shape, are locally curved in the direction of either the lowest or the highest bending stiffness. That is,

$$\boldsymbol{\kappa}^{(u)} = (K, 0, 0). \tag{21}$$

If $\mathbf{d}_1$ lies along the principal axis of inertia, $\Lambda \leq 1$, and the curvature is in the direction of lowest bending stiffness. This last assumption, while restrictive, seems natural as one expects a rod to be locally curved in the direction of lowest bending stiffness. Thus, the most common case would be the one in which $\Lambda \leq 1$, but we include the case $\Lambda \geq 1$ for greater generality.

In light of the discussion in the previous section, we can always rescale, by setting the length scale $L = K^{-1}$, the radius of the ring the rod forms in its unstressed state. This implies that $\boldsymbol{\kappa}^{(u)} = (1, 0, 0)$, and we can take $K = 1$ without loss of generality. However, in our analysis we leave K undefined, in order to make explicit the dependence of solutions on the intrinsic curvature.

In physical systems, there are various mechanisms for creating intrinsic curvature starting with an initially straight unstressed filament. For instance, *differential growth* is used in tendril perversion and in many other biological systems to curve strands [57]. Another mechanism is *heat setting* as used, for instance, in the textile industry where it is known as *false-twist technique* [58]. In this process, an initially straight filament is heated and shaped as a ring or helix and cooled down. Due to the thermoplasticity of many materials, the material conserves its new shape at lower temperature. Finally, in a common experiment, chemical unbonding and rebonding is performed on hair, in most salons, to artificially create curls. Again, this process is based on the simple idea of destroying certain chemical bonds and setting the filament in the desired shape where the bonds are then re-created (usually by both chemical and heat setting).

We now study how differential growth can affect the intrinsic curvature in the simplest case. Consider a filament initially of length $f(z)$ with $f(0) = 1$, where z is the cross-sectional width. Suppose the growth rate at width z is proportional to the length of the filament. The length as a function of t and z is then given by $L(z, t) = f(z)e^{kt}$. Since the filament is unshearable, the cross-sections remain at right angles to the edges and the curvature of the filament remains constant in time. The edges of the filament form circular arcs with radii r and R (see Fig. 7). The curvature κ of the entire filament is then $\kappa = (r + \frac{h}{2})^{-1}$. A simple computation shows that the curvature of the filament is $\kappa = 2[f(h) - 1]/(h[f(h) + 1])$. In the case of linear differential growth, $f(z) = az + 1$, we have $\kappa = [\frac{h}{2} + b]^{-1}$. Since we assume that the cross-section of the filament is small compared with the length, $h \ll 1$, the curvature is approximately $\kappa = a + \mathrm{O}(h)$.

In general, in biological material differential growth takes place in such a way that different points on the cross-sections experience different growth rates. This, in turn creates both intrinsic curvature and intrinsic twist that can vary with time and arclength. A complete treatment of the kinematics of differential growth requires a geometric description of each material line of the filaments and can be performed within the context of standard differential geometry [59].

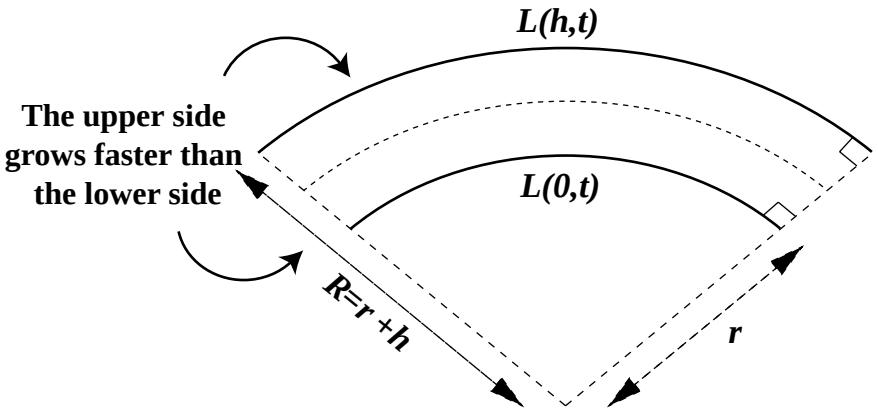

Fig. 7. Differential growth. The filament after growing for a time t. The dashed line is the central axis of the filament.

3. Static Solutions

We now seek solutions of the static equations (17–19). Forming the vector $\mathbf{X} = (F_1, F_2, F_3, \kappa_1, \kappa_2, \kappa_3)^T$, we obtain a system of six ordinary differential equations:

$$\mathbf{X}' = \mathbf{g}(\mathbf{X}). \tag{22}$$

We note that the system admits, for all values of the parameters Λ, Γ, and $\boldsymbol{\kappa}^{(u)}$, three first integrals:

$$I_1 = \kappa_1^2 + \Lambda\kappa_2^2 + \Gamma\kappa_3^2 + 2F_3, \tag{23}$$

$$I_2 = F_1^2 + F_2^2 + F_3^2, \tag{24}$$

$$I_3 = F_1(\kappa_1 - \kappa_1^{(u)}) + \Lambda F_2(\kappa_2 - \kappa_2^{(u)}) + \Gamma F_3(\kappa_3 - \kappa_3^{(u)}). \tag{25}$$

These first integrals represent, respectively, a local form of the energy, the force, and the inner product of the force with the moment. System (22) can be shown to be a Hamiltonian system with a noncanonical symplectic structure (similar to the one obtained by Mielke and Holmes [47]). It has three degrees of freedom with three first integrals (23–25). However, two of these integrals, namely (24–25) are so-called Casimirs and cannot be used directly to integrate the system following Poincaré-Arnold's theorem [60], [61]. They can be used to reduce the system to a four dimensional (two-degree of freedom) canonical Hamiltonian system with one first integral (the Hamiltonian itself). However, we have not been able to use this additional structure to our advantage and in the following we study the system using classical methods from dynamical systems.

In the case $\boldsymbol{\kappa}^{(u)} = K\mathbf{d}_1$, equation (22) reads

$$F_1' = F_2\kappa_3 - F_3\kappa_2, \tag{26}$$

$$F_2' = F_3\kappa_1 - F_1\kappa_3, \tag{27}$$

$$F_3' = F_1\kappa_2 - F_2\kappa_1, \tag{28}$$

$$\kappa_1' = F_2 + (\Lambda - \Gamma)\kappa_3\,\kappa_2, \tag{29}$$

$$\kappa_2' = -(F_1 + (1-\Gamma)\kappa_3\,\kappa_1 - K\,\kappa_3)/\Lambda, \tag{30}$$

$$\kappa_3' = ((1-\Lambda)\kappa_1\kappa_2 - K\kappa_2)/\Gamma. \tag{31}$$

The associated flow is invariant under two symmetries:

$$R_1\colon\ s \to -s,\ F_1 \to -F_1,\ F_2 \to -F_2,\ \kappa_3 \to -\kappa_3, \tag{32}$$

$$R_2\colon\ s \to -s,\ F_2 \to -F_2,\ \kappa_2 \to -\kappa_2. \tag{33}$$

We consider an ideal infinite filament, so that $s \in \mathbb{R}$. In this context, the space curve $\hat{\mathbf{x}} = \hat{\mathbf{x}}(s)$ representing a perversion approaches asymptotically helices with opposite handedness as $s \to \pm\infty$. Solutions in this case are bounded, and we therefore look for bounded solutions to (26–31), e.g., heteroclinic, homoclinic, or periodic orbits. As shown in the next section, helices of opposite handedness are different fixed points of the system (26–31). A perversion, in this setting, is thus a heteroclinic orbit.

3.1. Helical Solutions

A complete discussion of all fixed points of (26–31) is given in Appendix A where it is shown that all fixed points are either twistless helical solutions or twisted straight solutions. A *helix* is a curve with constant curvature κ and torsion τ. A helical solution represents a filament whose central axis is a helix. Therefore, all helical solutions have the form

$$\boldsymbol{\kappa} = (\kappa\sin(\zeta), \kappa\cos(\zeta), \tau + \zeta'), \tag{34}$$

where κ and τ are constant but ζ is, in general, a function of s. The twist is given by ζ', so that a *twistless helix* is one in which $\zeta' = 0$. We show in Appendix A that in order for a helical filament to be a stationary solution of (26–31) we must have $\zeta' = 0$ or $\kappa = 0$; therefore all helical filaments (excluding the straight helix) are twistless. Note however that the total twist (which includes torsion) of any section of a helix is not zero, it is just the pointwise twist density that is zero. Moreover, the helical solutions are such that

$$\boldsymbol{\kappa} = \kappa\mathbf{d}_1 + \tau\mathbf{d}_3, \tag{35}$$

$$\mathbf{F} = \gamma\tau\boldsymbol{\kappa}, \tag{36}$$

where $\gamma = (\frac{K}{\kappa} - 1 + \Gamma)$. This implies that the possible asymptotic helices in a perversion do not depend on the cross-section's characteristics, but only, as we now show, on the tension, intrinsic curvature, and Γ, the ratio of twisting to bending stiffness.

The tension applied at the ends of a rod forming a perversion is applied along the *axes* of the asymptotic helices. The *axis of a helix* is the centerline of the cylinder around which a helix is wrapped. This is not to be confused with the axis of a rod, which is the centerline of a rod. In order to compute the force in the direction of the axis of the asymptotic helices, we compute the force in terms of a fixed frame of reference. Let $(\mathbf{e}_1, \mathbf{e}_2, \mathbf{e}_3)$ be a fixed Euclidean basis, where $\mathbf{e}_3$ is chosen to lie along the axis of the asymptotic helices of a perversion. The external tension is then applied along $\mathbf{e}_3$, and, in

order to compute the applied external force in terms of the components of $\mathbf{F}$, we calculate the component of the force vector in this direction. A helix with curvature κ and torsion τ, with axis along $\mathbf{e}_3$, can be written

$$\mathbf{x}(s) = \frac{\kappa}{\lambda^2}\cos(\lambda s)\,\mathbf{e}_1 + \frac{\kappa}{\lambda^2}\sin(\lambda s)\,\mathbf{e}_2 + \frac{\tau}{\lambda}s\,\mathbf{e}_3, \tag{37}$$

where $\lambda = \sqrt{\kappa^2 + \tau^2}$. Since helical filaments have no twist, we can write the director basis $(\mathbf{d}_1, \mathbf{d}_2, \mathbf{d}_3)$ in terms of the Frenet basis $(\mathbf{n}, \mathbf{b}, \mathbf{t})$, determined by (5). Substituting the twist vector $\boldsymbol{\kappa} = \kappa\mathbf{d}_1 + \tau\mathbf{d}_3$ into the twist equations (3), the equations for the basis vectors are

$$\mathbf{d}_1' = \tau\,\mathbf{d}_2, \tag{38}$$

$$\mathbf{d}_2' = \kappa\,\mathbf{d}_3 - \tau\,\mathbf{d}_1, \tag{39}$$

$$\mathbf{d}_3' = -\kappa\,\mathbf{d}_2. \tag{40}$$

Using (5), and the fact that $\mathbf{d}_3 = \mathbf{t}$, equations (38–40) are solved by

$$\mathbf{d}_1 = \mathbf{b}, \qquad \mathbf{d}_2 = -\mathbf{n}, \qquad \mathbf{d}_3 = \mathbf{t}. \tag{41}$$

Hence, we can calculate $(\mathbf{d}_1, \mathbf{d}_2, \mathbf{d}_3)$ in terms of the Euclidean basis using (5),

$$\mathbf{d}_1 = \frac{1}{\lambda}(\tau\sin(\lambda s)\,\mathbf{e}_1 - \tau\cos(\lambda s)\,\mathbf{e}_2 + \kappa\,\mathbf{e}_3), \tag{42}$$

$$\mathbf{d}_2 = \cos(\lambda s)\,\mathbf{e}_1 + \sin(\lambda s)\,\mathbf{e}_2, \tag{43}$$

$$\mathbf{d}_3 = \frac{1}{\lambda}(-\kappa\sin(\lambda s)\,\mathbf{e}_1 + \kappa\cos(\lambda s)\,\mathbf{e}_2 + \tau\,\mathbf{e}_3). \tag{44}$$

Thus, the force in the Euclidean basis is

$$\begin{aligned}\mathbf{F} &= F_1\mathbf{d}_1 + F_2\mathbf{d}_2 + F_3\mathbf{d}_3 \\ &= \frac{1}{\lambda}[\lambda\,\cos(\lambda s)\,F_2 + \tau\,\sin(\lambda s)\,F_1 - \kappa\,\sin(\lambda s)F_3]\,\mathbf{e}_1 \\ &\quad + \frac{1}{\lambda}[\lambda\,\sin(\lambda s)F_2 - \tau\,\cos(\lambda s)F_1 + \kappa\,\cos(\lambda s)F_3]\,\mathbf{e}_2 + \frac{1}{\lambda}[\tau F_3 + \kappa F_1]\mathbf{e}_3,\end{aligned} \tag{45}$$

where the F_j's are s-independent. Note that the external tension is given by $T = \frac{1}{\lambda}[\tau\,F_3 + \kappa\,F_1]$.

3.2. Asymptotic States

We now identify among the two-parameter family of helical solutions (given by curvature and torsion), a one-parameter family of solutions formed by the asymptotic states of heteroclinic solutions. A *perversion*, $\hat{\boldsymbol{\kappa}} = \hat{\boldsymbol{\kappa}}(s)$, is a heteroclinic solution that connects asymptotically two helices with the same curvature κ but opposite torsion τ, that is

$$\hat{\boldsymbol{\kappa}} \underset{s\to\pm\infty}{\to} \kappa\mathbf{d}_1 \pm \tau\mathbf{d}_3. \tag{46}$$

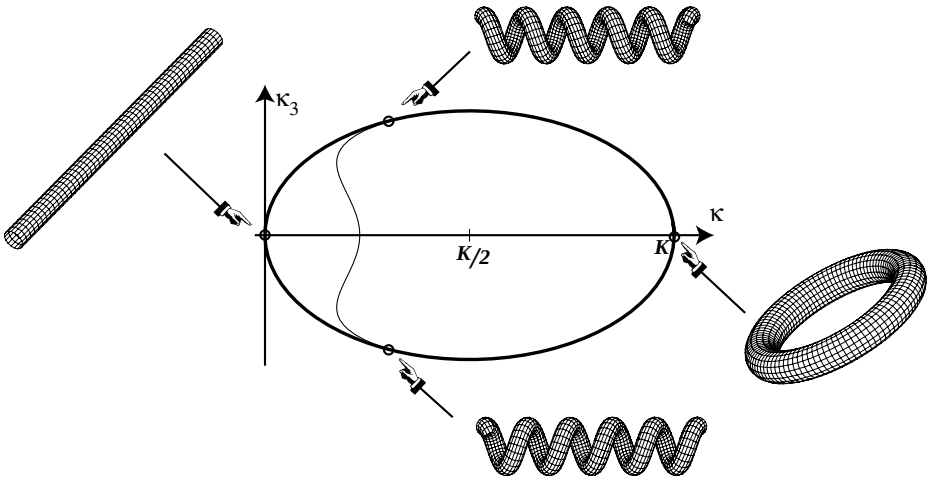

Fig. 8. The set of helices that can connect asymptotically to another helix with opposite torsion forms an ellipse in the curvature–torsion plane.

Thus, on this solution we can calculate the first integrals in terms of the parameters and the tension. Substituting (35–36) into the first integrals (23–25), we obtain

$$I_1 = \kappa^2 + (\Gamma + 2\gamma)\tau^2, \tag{47}$$

$$I_2 = \gamma^2\tau^2(\kappa^2 + \tau^2), \tag{48}$$

$$I_3 = \tau\gamma[\Gamma\tau^2 - \kappa(K - \kappa)]. \tag{49}$$

We note that I_1 and I_2 are even in τ, while I_3 is odd in τ. Therefore, on the two asymptotic fixed points, we have $I_3(\tau) = -I_3(\tau)$, which implies $I_3 = 0$. Thus, in the curvature–torsion plane, the set of possible asymptotic helices form the ellipse

$$\left(\kappa - \frac{K}{2}\right)^2 + \Gamma\tau^2 = \frac{K^2}{4}. \tag{50}$$

A perversion is a heteroclinic orbit connecting two points on this ellipse, as seen in Figure 8. Now, we solve for the asymptotic curvature and torsion in terms of the tension and parameters of the system. The external force is applied at the ends of the filament. Without loss of generality, we assume that $\tau > 0$. The other asymptotic helix then has torsion $-\tau$. We call the force at the ends $T = \mathbf{F}.\mathbf{e}_3$, the applied tension, which is applied along the axis of the asymptotic helices. That is, T is the magnitude of the applied tension, which is applied in opposite directions at $s = \pm\infty$. Substituting (36) into the z component of the force, and identifying it with the tension, we have another equation for the curvature and torsion:

$$T = \gamma\tau\lambda. \tag{51}$$

The previous equation, along with (50), allows us to solve for κ and τ in terms of the parameters and the applied tension. The following equation for κ can be derived by

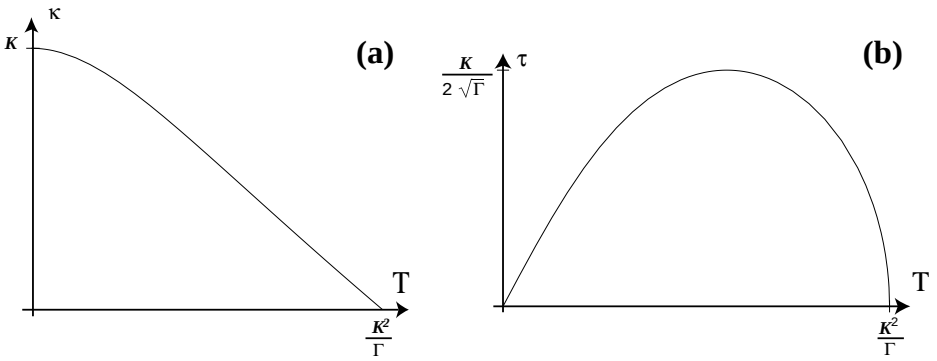

Fig. 9. Asymptotic helices. (a) The curvature, and (b) the torsion of the asymptotic helices in a perversion, as functions of the applied tension.

solving for τ^2 and substituting into (51):

$$[K-\kappa(1-\Gamma)]^3\,(K-\kappa)=\Gamma^2\,T^2. \tag{52}$$

Equation (52) is a fourth-degree polynomial equation for κ for which there is exactly one real solution in $0<\kappa<K$, the physically relevant case, for $0<T<K^2/\Gamma$. The asymptotic curvature κ varies monotonically from K to 0 as the tension T varies from 0 to K^2/Γ. The tension $T=K^2/\Gamma$ is the critical tension above which the solution representing a perversion does not exist. At $T=0$, the filament is a ring with radius K^{-1}, and for $T\geq K^2/\Gamma$ the filament is straight. The curvature as a function of the tension is obtained by solving (52) and is seen in Figure 9a. Furthermore, the first integrals are

$$I_1 \;=\; 2\frac{K^2}{\Gamma}+\left(3-\frac{4}{\Gamma}\right)K\kappa+\frac{2}{\Gamma}(1-\Gamma)\kappa^2, \tag{53}$$

$$I_2 \;=\; T^2, \tag{54}$$

$$I_3 \;=\; 0, \tag{55}$$

where κ is given by the solution of (52).

We can now deduce the boundary conditions necessary to produce a perversion solution as we have defined it. We have defined a perversion in an idealized form as a heteroclinic orbit. In this setting, for a rod with intrinsic curvature K in the direction $\mathbf{d}_1$, and a tension T applied at the ends at $\pm\infty$, the boundary conditions are given by the asymptotic condition (46). If the tension is positive, then the curvature of the asymptotic helices is different from the intrinsic curvature. The control parameter in the problem is the tension T. From the previous analysis, once T is given, one can obtain the asymptotic curvature κ and torsions $\pm\tau$. Therefore, the moment and force at infinity are given by

$$\mathbf{M}=(\kappa-K)\mathbf{d}_1\pm\Gamma\tau\mathbf{d}_3, \tag{56}$$

$$\mathbf{F}=\gamma\tau\boldsymbol{\kappa}, \tag{57}$$

where γ and $\boldsymbol{\kappa}$ are defined in (35). Physically, when a rod is held straight and the tension slowly released, a moment must be applied at the ends in order to keep the ends from

rotating. The condition for a perversion solution is that the total twist is zero, which is equivalent to the condition that the ends do not rotate as the tension is released.

Clearly, these infinite homoclinic orbits are not physical solutions in the sense that there is no infinite filament. However, we show that the heteroclinic solution approaches the asymptotic helices exponentially fast (in arclength) so that a finite piece of a heteroclinic orbit symmetric with respect to torsion gets so close to the limiting helix solutions that boundary conditions would be close to those of a finite rod. Moreover, the normal form analysis performed in this paper reveals the existence of a family of periodic orbits with arbitrary period converging to the heteroclinic orbit. These solutions can be matched to specific symmetric boundary conditions for finite-length perversion solutions.

3.3. Spring Characteristics

A perversion in a rod makes a *twistless spring*, a spring with zero total twist. The characteristics of the spring, i.e., the Hooke's constant, can be calculated in terms of the properties of the material from which the rod is made: its Young's modulus and Poisson ratio. In particular, we can calculate how much a spring formed by a perversion deviates from Hooke's law, $F = hx$, for an ideal spring where x is the distance along the axis of the spring. In this section, we compare the characteristics of a spring made from a perversion to a spring made from a helix. We first discuss the properties of a spring made from a perversion.

Consider a rod with intrinsic curvature K in the direction $\mathbf{d}_1$. When no tension is applied to the rod, the rod forms a ring of radius $2\pi/K$. We can consider this state to be the natural state of the rod, even though for a rod with a finite radius, the rod can never obtain the ring shape, as self-contact would prevent tight packing. The diameter of the rod is taken into account in the next section. When a tension T is applied at the ends of the rod, in the direction of the axis of the helix (normal to the plane the ring lies in when no tension is applied), the rod forms a perversion. We calculate the length the spring is stretched by a tension T in the direction of the axes of the asymptotic helices. Consider the unstretched ring, and two material points $\mathbf{P}_1$ and $\mathbf{P}_2$ on successive rings. In the unstretched state, $\mathbf{P}_1$ and $\mathbf{P}_2$ occupy the same point in space. When tension is applied, the points separate as two asymptotic helices are created, connected by the perversion (Fig. 10). We assume that the points $\mathbf{P}_1$, $\mathbf{P}_2$ lie on the same asymptotic helix given by

$$\mathbf{x}(s) = \frac{1}{\lambda^2}(\kappa\cos(\lambda s), \kappa\sin(\lambda s), \tau\lambda s). \tag{58}$$

Taking $\mathbf{P}_1 = \mathbf{x}(0)$, we have $\mathbf{P}_2 = \mathbf{x}(2\pi/K)$. The distance d between the z-coordinates of $\mathbf{P}_1$ and $\mathbf{P}_2$ is $d = 2\pi\tau/\lambda K$. Using the condition that the curvature and torsion lie on the ellipse (50), d is given by

$$d = \frac{2\pi}{K}\sqrt{\frac{K-\kappa}{K-\kappa(1-\Gamma)}}. \tag{59}$$

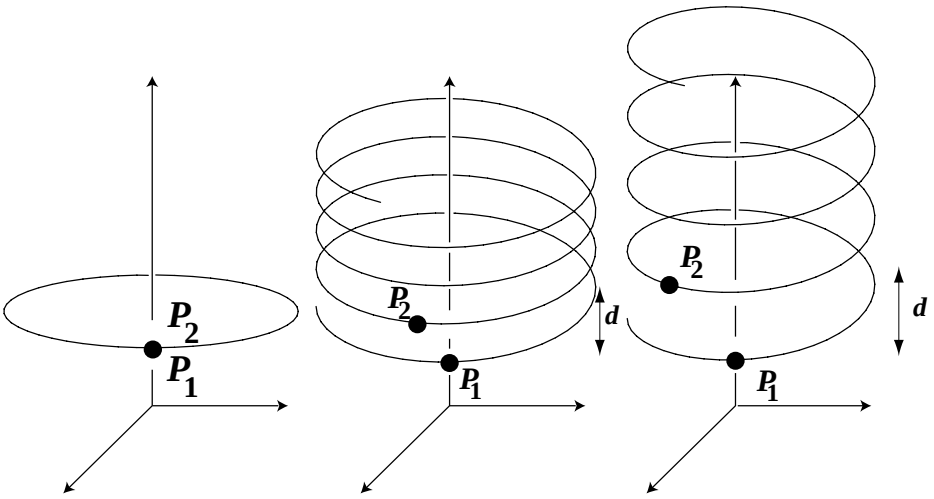

Fig. 10. The stretch of asymptotic helices in a perversion under tension. The points P_1 and P_2 are identified on the multicovered ring (left). The helix is stretched in such a way that these two points remain along the same vertical axis (middle and right pictures).

Solving for κ, and using the relation (52) between the tension T and κ, the relation between the tension and d is

$$T = \frac{K^3\Gamma}{2\pi}\frac{d}{\left(1 - d^2\frac{K^2(1-\Gamma)}{4\pi^2}\right)^2}. \tag{60}$$

This relation can be expressed in terms of the unscaled variables. Recall that the force and intrinsic curvature were scaled by

$$\mathbf{F} \to \frac{EI_1}{L^2}\mathbf{F}, \qquad \boldsymbol{\kappa}^{(u)} \to L^{-1}\,\boldsymbol{\kappa}^{(u)}, \tag{61}$$

where L is the length scale. We call the unscaled tension $\tilde{T}$, and the unscaled intrinsic curvature in the direction $\mathbf{d}_1$, $\tilde{K}$. By the preceding scalings, we see that

$$T = \frac{L^2}{E\,I_1}\,\tilde{T}, \qquad K = L\,\tilde{K}. \tag{62}$$

Making these substitutions, choosing the length scale to be $L = 2\pi/K$, and dropping the tildes, the relation between the unscaled tension and d becomes

$$T = h\frac{d}{(1 - d^2(1-\Gamma))^2}, \tag{63}$$

where $h = K^2\,\Gamma\,EI_1 = 4\,\pi^2\,\Gamma\,EI_1$. The length l of the rod in the z-direction is $l = nd$, where n is the number of rings in the unstressed rod. Therefore, d is the ratio of the length of the rod in the z-direction to the length of the fully stretched, straight rod. Since

the circumference of a ring is 1, n is also the length of the fully stretched straight rod and $0 \le d \le 1$. Thus (63) gives the relation between the tension and the fractional length of the spring. To third order, (63) reads

$$T = hd + 2\,hd^3\,(1-\Gamma) + \mathrm{O}(d^5). \tag{64}$$

Since $0 \le (1-\Gamma) \le 1/3$ and $0 \le d \le 1$, the deviation of this relation from Hooke's law is very small for small d. However, as the rod is stretched to near its full length, $d \to 1$ and the cubic term dominates. The tension T varies from 0 to h/Γ^2 as d varies from 0 to 1, in contrast to the ideal spring, in which the tension varies from 0 to h. Note that as $\Gamma \to 1$, or as the material gets stiffer, the elastic properties of a perversion spring approach those of an ideal spring.

Now, we calculate the properties of springs made of helices. Consider a rod that is helical in its unstressed state $\boldsymbol{\kappa}^{(u)} = K\,\mathbf{d}_1 + \tau_0\,\mathbf{d}_3$. Consider the case similar to that of the spring made of a perversion, in which the ends are held so that they do not rotate as the tension is changed, where the tension is applied at the ends in the direction of the axis of the helix. While the ends are held so that they do not rotate, a moment must be applied to the ends. As tension is applied, the helix deforms to a new helix with curvature κ and torsion τ. Not allowing the ends to rotate imposes the constraint that the total twist is constant:

$$Tw = \int \kappa_3 ds = \int \tau_0 ds = \int \tau ds. \tag{65}$$

This constrains the torsion τ to remain constant, that is, $\tau = \tau_0$. The relation (51) holds (with the corresponding value of γ given in Appendix A), and the tension is given by

$$T = \gamma\,\tau\,\lambda = \left(\frac{K}{\kappa} - 1\right)\tau_0\lambda_0, \tag{66}$$

where $\lambda_0^2 = K^2 + \tau_0^2$. As before, we look at the distance of two material points in the direction of the axis of the helix. Letting $\mathbf{P}_1, \mathbf{P}_2$ be two points on successive rings when no tension is applied, and choosing $\mathbf{P}_1 = \mathbf{x}(0)$, then $\mathbf{P}_2 = \mathbf{x}(2\pi/\lambda_0)$. The distance d along the helical axis between the two material points is thus

$$d = \frac{2\,\pi\,\tau}{\lambda\lambda_0}. \tag{67}$$

Converting to unscaled variables,

$$T \to \frac{L^2}{E\,I_1}\,T, \qquad K \to L\,K, \qquad \tau \to L\,\tau, \tag{68}$$

and choosing the length scale to be the arclength between $\mathbf{P}_1$ and $\mathbf{P}_2$, $L = 2\pi/\lambda_0$, the unscaled relation between the tension and d is

$$T = E\,I_1\left(\frac{K\,\tau}{\sqrt{1-d^2}} - \frac{\tau^2}{d}\right). \tag{69}$$

Now, in the unstressed state, $d = d_0 = \tau_0/\lambda_0$. We see that T varies from 0 to ∞ as d varies from d_0 to 1. Let $d = d_0 + \hat{d}$. Then

$$T = h\,\hat{d} + \mathrm{O}(\hat{d}^2), \tag{70}$$

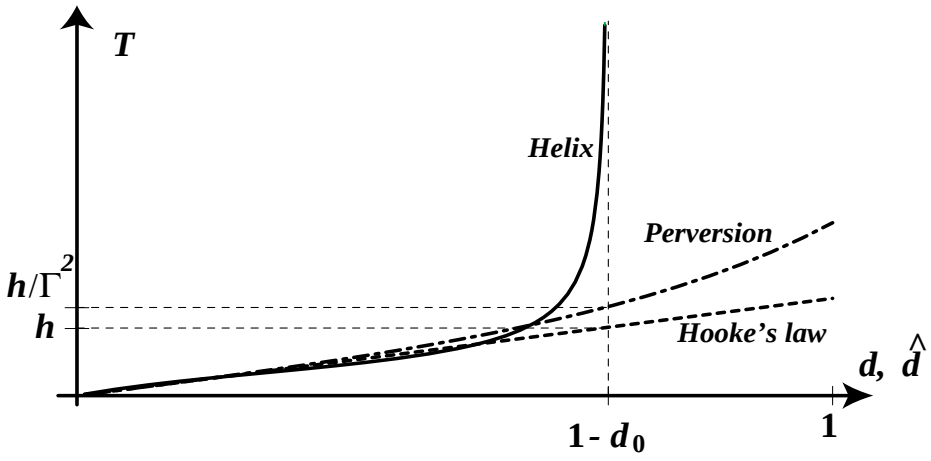

Fig. 11. Comparison of springs made of perversions and helices. The dash-dot curve is the plot of the tension T versus the distance d for a perversion. The solid curve is the plot of the tension T vs. $\hat{d}$ for a helical spring. The dashed curve is the plot of the tension vs. the displacement for an ideal spring (Hooke's law).

where, since $L = 2\pi/\lambda_0$,

$$h = EI_1 4\pi^2 \left(1 + 4\pi^2 \frac{\tau_0^2}{K^2}\right). \tag{71}$$

As before, the Hooke's constant for small tension is proportional to EI_1, but larger than that for the spring made of a perversion. We also note that in the case of the helical spring $T \to \infty$ as $d \to 1$. Thus, a helical spring is stiffer than a spring made of a perversion. See Figure 11 for a comparison of the characteristics of springs formed by perversions and helices.

3.4. Self-contact

The curvature and torsion of a helix are further limited by the diameter D of the rod. The additional constraints arise from the conditions that *(i)* consecutive cross-sections of the rod cannot overlap, and *(ii)* the helix can only be packed as close as self-contact of successive turns of the helix allows. The constraint that consecutive cross-sections of a rod do not overlap is expressed by constraining the curvature below the reciprocal radius of the rod:

$$\kappa \leq \frac{2}{D}. \tag{72}$$

We note that this constraint applies to all points on a filament, and not just to helical solutions. The second constraint, that successive turns of the helix do not intersect, is derived here in terms of κ and τ, following the derivation in [62]. The helix and tangent

vectors are given, as before, by

$$\mathbf{x}(s) = \frac{1}{\lambda^2}(\kappa\cos(\lambda s), \kappa\sin(\lambda s), \tau\kappa s), \tag{73}$$

$$\mathbf{t}(s) = \frac{1}{\lambda}(-\kappa\sin(\lambda s), \kappa\cos(\lambda s), \tau). \tag{74}$$

Consider a helical rod whose consecutive turns are in contact. Chose a point $\mathbf{P_1}$, taken at $s = 0$. In order for the turns of the helix to touch each other, the minimum distance of $\mathbf{P_1}$ to the points on the next turn of the helix must equal D. Let $\mathbf{P_2}$ be the point at which this minimum distance is reached, and $\mathbf{t_1}$, $\mathbf{t_2}$ the tangent vectors at $\mathbf{P_1}$ and $\mathbf{P_2}$. Then

$$\mathbf{P_1} = \left(\frac{\kappa}{\lambda^2}, 0, 0\right), \tag{75}$$

$$\mathbf{t_1} = \left(0, \frac{\kappa}{\lambda}, \frac{\tau}{\lambda}\right). \tag{76}$$

The vector $\mathbf{P_{12}} = \mathbf{P_2} - \mathbf{P_1}$ is perpendicular to both $\mathbf{t_1}$ and $\mathbf{t_2}$. Let Σ_1 be the plane through the point $\mathbf{P_1}$ and perpendicular to the tangent vector $\mathbf{t_1}$, and similarly for Σ_2. Then $\mathbf{P_{12}}$ lies on the line of intersection of Σ_1 and Σ_2. The plane Σ_1 is defined by the equation

$$\kappa\, y + \tau\, z = 0. \tag{77}$$

Let ξ be the value of the arclength s such that $\mathbf{P_2} = \mathbf{x}(\xi)$. Since $\mathbf{P_2}$ lies on Σ_1,

$$\frac{\kappa^2}{\lambda^2}\sin(\lambda\xi) + \frac{\tau^2}{\lambda}\xi = 0. \tag{78}$$

Setting $|\mathbf{P_{12}}| = D$, we have

$$2\frac{\kappa^2}{\lambda^2}(1 - \cos(\lambda\xi)) + \tau^2\xi^2 = D^2\lambda^2. \tag{79}$$

Setting $\xi' = \lambda\xi$, equations (78) and (79) become

$$2\,\kappa^2(1 - \cos(\xi')) + \tau^2\xi'^2 = D^2(\kappa^2 + \tau^2)^2, \tag{80}$$

$$\kappa^2\,\sin(\xi') + \tau^2\xi' = 0. \tag{81}$$

This system is solved for κ and τ,

$$\kappa = \sqrt{\frac{\xi^2[2(1 - \cos(\xi')) - \xi'\,\sin(\xi')]}{D^2\,(\xi' - \sin(\xi'))^2}}, \tag{82}$$

$$\tau = \pm\sqrt{\frac{\xi'\,\sin(\xi')[2(\cos(\xi') - 1) + \xi'\sin(\xi')]}{D^2\,(\xi' - \sin(\xi'))^2}}. \tag{83}$$

Equations (82–83) describe parameterically a curve in the $\kappa - \tau$ plane. This curve is seen in Figure 12a. The curve defined by (82–83) is the solid curve and has two branches (for each sign of τ). The upper branch is the physically relevant branch. This curve represents,

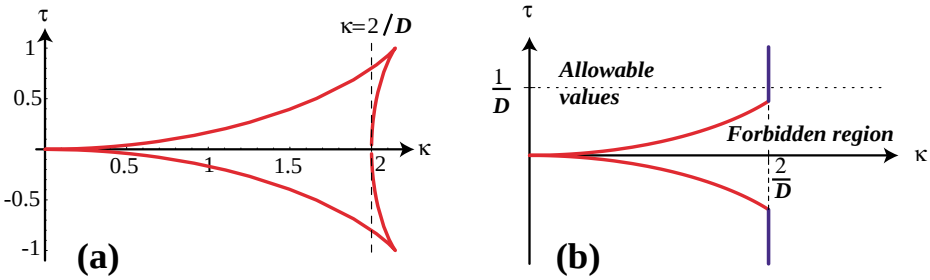

Fig. 12. Allowable values of the curvature and torsion of a helical rod. (a) The curves delimiting the two conditions of nonintersection of successive turns of a helix and nonintersection of successive cross-sections of a rod. (b) The allowed values in the $\kappa - \tau$ plane.

for a given diameter of the rod D, helices whose successive turns are in contact. Thus, for a given value of τ, κ must lie to the left of this curve (or on the curve) in order that successive turns of the helix do not overlap.

Combining this constraint with the local curvature condition $\kappa \leq 2/D$, we obtain a curve in the $\kappa - \tau$ plane, which separates the allowable helices from the forbidden region, as seen in Figure 12b. We emphasize again that the condition that (κ, τ) lie to the left of the curve defined in (82–83) applies only to the asymptotic helices in a perversion solution, whereas the condition $\kappa \leq 2/D$ applies to every point of an orbit which solves the Kirchhoff equations.

Further, we note that the cusp points of Figures 12a–b represent the *optimal helices* of Maritan et al. [63], that is, closely packed helices with minimal curvature.

For a rod with diameter D, the value at which the rod becomes tightly packed, or at which self-contact prevents further coiling, gives a maximum value of the curvature of the asymptotic helices (Fig. 13). In turn, this gives a minimum value of the tension T at which the perversion reaches this state (see Fig. 14).

4. Reduction to the Center Manifold

Now that we have determined the type of asymptotic solutions allowed by the equations and the qualitative behavior of the solutions, we turn to an analysis of the static Kirchhoff equations (26–31). We treat these equations in the context of dynamical systems, in which the arclength s plays the role of time. We calculate the center manifold on which the perversion solution lies, and then compute the normal form of the center manifold equations. This analysis of this simplified system provides us with a complete description of the solutions close to the bifurcation point.

The linearized equations of system (26–31) around the fixed point $\mathbf{X}^* = (0, 0, \phi^2, 0, 0, 0)$ representing a straight, untwisted rod under tension $T = \phi^2$, has linear eigenvalues

$$0, \qquad \pm\phi, \qquad \text{and} \qquad \pm\sqrt{\phi^2 - \frac{K^2}{\Gamma}}. \tag{84}$$

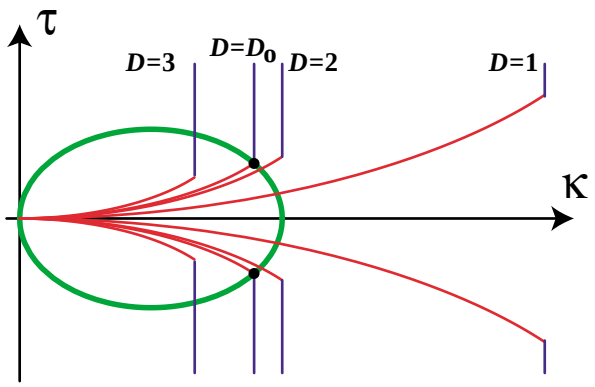

Fig. 13. The boundary of allowed values in the $\kappa - \tau$ plane for four values of the diameter of the rod, along with the ellipse of possible values of κ and τ in the asymptotic helices of a perversion. The optimal helices lying on the ellipse of allowed helices are marked with a dot. In this case $D_0 \approx 2.24$, that is, the critical diameter is about twice the reciprocal of the intrinsic curvature.

At the critical tension $\phi_c^2 = K^2/\Gamma$, two eigenvalues coalesce and a Hamiltonian pitchfork bifurcation occurs. This is the critical value below which the perversion solution exists. A dynamical analysis of the Kirchhoff equations (17–19) was performed in [7], where it was revealed that for $\phi < \phi_c$, the straight filament with intrinsic curvature is temporally unstable. We can therefore study the phenomenon of perversion near this critical value of the tension as a bifurcation problem.

We examine the bifurcation at $\phi = \phi_c$ by using the first integrals (53) and (55) to reduce the dimension of the system by two. The resulting system is then reduced to the center manifold of the fixed point, and a simplified system is derived which governs the dynamics. The perversion solution lies on the center manifold of the fixed point X^*.

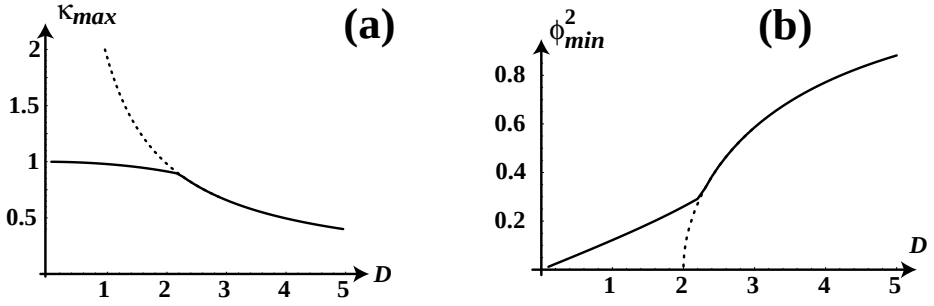

Fig. 14. The maximum curvature (a) and minimum tension (b) of the asymptotic helices before self-contact or overlapping occurs. The cusps in the graphs represent optimal helices. The dashed curve in (a) is the plot of $2/D$. The dashed curve in (b) is the plot of the tension with the curvature set to $2/D$. Values of the parameters are $K = 1, \Gamma = 3/4, \Lambda = 1$.

Therefore, we look at solutions around the point X^* for tension just below the critical tension. First, we use the first integrals to reduce the dimension of the system by two. We could, in principle, reduce the dimension by three, but this cannot be achieved globally. Using (23) and (25), we solve for F_1 and F_3 in terms of F_2 and $\boldsymbol{\kappa}$. Substitution into the system (26–31) yields the following reduced system:

$$F_2' = \frac{\kappa_1}{2}\left(I_1 - {\kappa_1}^2 - \Lambda{\kappa_2}^2 - \Gamma\,{\kappa_3}^2\right) + \frac{\kappa_3(2I_3 - 2\Lambda\,F_2\,\kappa_2 + \Gamma\,\kappa_3\,(-I_1 + {\kappa_1}^2 + \Lambda{\kappa_2}^2 + \Gamma\,{\kappa_3}^2))}{2(K - \kappa_1)}, \tag{85}$$

$$\kappa_1' = F_2 + (\Lambda - \Gamma)\,\kappa_2\,\kappa_3, \tag{86}$$

$$\kappa_2' = \frac{2I_3 - 2\Lambda F_2\kappa_2 + \kappa_3(2K^2 - I_1\Gamma - 2K(2-\Gamma)\kappa_1 + (2-\Gamma){\kappa_1}^2 + \Gamma\Lambda{\kappa_2}^2 + \Gamma^2{\kappa_3}^2)}{2\Lambda(K - \kappa_1)}, \tag{87}$$

$$\kappa_3' = -\frac{K}{\Gamma}\kappa_2 + (1 - \Lambda)\kappa_1\kappa_2. \tag{88}$$

The solution representing a perversion solves (85–88) with $I_3 = 0$. The first integral I_1 depends on the parameters by (53). Substituting these values of I_1, I_3 into (85–88), we study solutions near the bifurcation, that is, for values of the tension just below the critical tension. We introduce the *distance to the bifurcation* $\mu \equiv \phi - \phi_c = \phi - K/\sqrt{\Gamma}$, where μ is taken to be small and negative, and consider the extended system

$$\mathbf{X}' = \mathbf{A}\mathbf{X} + \mathbf{f}(\mathbf{X}), \tag{89}$$

where $\mathbf{X} = (F_2, \kappa_1, \kappa_2, \kappa_3, \mu)^T$,

$$\mathbf{A} = \begin{pmatrix} 0 & K^2/\Gamma & 0 & 0 & 0 \\ 1 & 0 & 0 & 0 & 0 \\ 0 & 0 & 0 & 0 & 0 \\ 0 & 0 & -K/\Gamma & 0 & 0 \\ 0 & 0 & 0 & 0 & 0 \end{pmatrix}, \tag{90}$$

and f contains only nonlinear terms in $\mathbf{X}$. At the critical tension, $\mu = 0$, the curvature is zero, so $I_1 = 2K^2/\Gamma$. For small μ, we expand I_1 in μ:

$$I_1 = \frac{2\,K^2}{\Gamma} + i_1\mu + i_2\mu^2 + \cdots, \tag{91}$$

where the coefficients i_j are functions of the parameters. We find a matrix S such that $\mathbf{S}^{-1}\mathbf{A}\mathbf{S} = \mathbf{J}$ is in Jordan form. Setting $\mathbf{X} = \mathbf{S}\mathbf{Y}$, we obtain the transformed system

$$\mathbf{Y}' = \mathbf{J}\mathbf{Y} + \mathbf{g}(\mathbf{Y}), \tag{92}$$

where $\mathbf{g}(\mathbf{Y}) = \mathbf{S}^{-1}\mathbf{f}(\mathbf{S}\mathbf{Y})$, and

$$\mathbf{J} = \begin{pmatrix} 0 & 0 & 0 & 0 & 0 \\ 0 & 0 & 1 & 0 & 0 \\ 0 & 0 & 0 & 0 & 0 \\ 0 & 0 & 0 & -K/\sqrt{\Gamma} & 0 \\ 0 & 0 & 0 & 0 & K/\sqrt{\Gamma} \end{pmatrix},$$

$$\mathbf{S} = \begin{pmatrix} 0 & 0 & 0 & -K/\sqrt{\Gamma} & K/\sqrt{\Gamma} \\ 0 & 0 & 0 & 1 & 1 \\ 0 & 0 & -\Gamma/K & 0 & 0 \\ 0 & 1 & 0 & 0 & 0 \\ 1 & 0 & 0 & 0 & 0 \end{pmatrix}. \tag{93}$$

System (92) can be written

$$\mathbf{W}' = \mathbf{J_1}\,\mathbf{W} + \mathbf{G_1}(\mathbf{W}, \mathbf{Z}), \tag{94}$$

$$\mathbf{Z}' = \mathbf{J_2}\,\mathbf{Z} + \mathbf{G_2}(\mathbf{W}, \mathbf{Z}), \tag{95}$$

where $\mathbf{W} = (y_1, y_2, y_3)^T$, $\mathbf{Z} = (y_6, y_7)^T$, and

$$\mathbf{J_1} = \begin{pmatrix} 0 & 0 & 0 \\ 0 & 0 & 1 \\ 0 & 0 & 0 \end{pmatrix}, \qquad \mathbf{J_2} = \begin{pmatrix} -\frac{K}{\sqrt{\Gamma}} & 0 \\ 0 & \frac{K}{\sqrt{\Gamma}} \end{pmatrix}. \tag{96}$$

Next, we derive the approximate equations for the flow on the center manifold. The analytic center manifold tangent to the center subspace $\mathbf{Z} = \mathbf{0}$ is

$$\mathbf{Z} = \mathbf{H}(\mathbf{W}) = \mathbf{H}^{(2)}(\mathbf{W}) + \mathbf{H}^{(3)}(\mathbf{W}) + \cdots,$$

where $\mathbf{H}^{(k)}(\mathbf{W})$ is a homogeneous polynomial of degree k in $\mathbf{W}$ obtained by the usual technique of center manifold reduction [64], [65]. In our case, we have

$$\mathbf{H}^{(2)}(\mathbf{W}) = \frac{\Gamma}{2K^3} \begin{pmatrix} K^2 {y_2}^2 - K(2+\Lambda-\Gamma)\sqrt{\Gamma}\, y_2 y_3 + (2+\Lambda-\Gamma)\Gamma {y_3}^2 \\ K^2 {y_2}^2 + K(2+\Lambda-\Gamma)\sqrt{\Gamma}\, y_2 y_3 + (2+\Lambda-\Gamma)\Gamma {y_3}^2 \end{pmatrix}, \tag{97}$$

and the center manifold equations, to fourth order, are

$$x' = y(1 - \alpha_1 x^2 - \beta_1 y^2), \tag{98}$$

$$y' = x(-\psi + \alpha_2 x^2 + \beta_2 y^2), \tag{99}$$

where $x = y_2$ and $y = y_3$, and the third equation reads $\mu' = 0$. The constants ψ, α_i, and β_i are positive functions of the parameters (for $\mu < 0$):

$$\alpha_1 = \frac{\Gamma}{K^2}(1-\Lambda), \tag{100}$$

$$\beta_1 = \frac{\Gamma^2}{K^4}(1-\Lambda)(2+\Lambda-\Gamma), \tag{101}$$

$$\psi = -\frac{1}{2}(i_1\mu + i_2\mu^2), \tag{102}$$

$$\alpha_2 = \frac{1}{2\Lambda}(4-3\Gamma), \tag{103}$$

$$\beta_2 = \frac{\Gamma}{2\Lambda K^2}(2\Gamma^2 - (8+\Lambda)\Gamma + 2(4-\Lambda^2)). \tag{104}$$

5. Analysis of the Reduced System

5.1. The Symmetric Case

In the symmetric case, $\Lambda = 1$, when the principal moments of inertia of the cross-section are equal (e.g., when the cross-section is circular), the center manifold equations (98–99) simplify to

$$x' = y, \tag{105}$$

$$y' = x[-\psi + \alpha x^2 + \beta y^2], \tag{106}$$

or, equivalently,

$$x'' = x[-\psi + \alpha x^2 + \beta (x')^2], \tag{107}$$

where $\alpha = \alpha_2,\ \beta = \beta_2$, with $\Lambda = 1$. The fixed points of the system are

$$(0, 0), \qquad \left(\sqrt{\frac{\psi}{\alpha}}, 0\right), \qquad \text{and} \qquad \left(-\sqrt{\frac{\psi}{\alpha}}, 0\right). \tag{108}$$

In terms of the original variables, the first fixed point represents a straight filament, while the second and third represent helices with equal but opposite handedness. The perversion is thus represented by a heteroclinic orbit connecting the second and third fixed points. Notice that $\psi(\mu = 0) = 0$, so that the fixed points representing the helices bifurcate from zero as μ goes through zero. Again, as the tension decreases through ϕ_c^2, two asymptotic helices are created.

The system (105–106) has the following first integral:

$$I = \left[y^2 + \frac{\alpha}{\beta}x^2 + \frac{\alpha - \beta\psi}{\beta^2}\right] e^{-\beta x^2}. \tag{109}$$

On the heteroclinic orbit representing a perversion, the first integral I must be constant on the two points it connects, i.e.,

$$I\left(x = \sqrt{\psi/\alpha}, y = 0\right) = I\left(x = -\sqrt{\psi/\alpha}, y = 0\right). \tag{110}$$

This implies that

$$I = \frac{\alpha}{\beta^2} e^{-\beta\psi/\alpha}. \tag{111}$$

We can thus solve for y and obtain a parameterization of the solution representing a perversion:

$$y = \pm\left[\frac{\alpha}{\beta^2}\left(e^{\beta(x^2 - \psi/\alpha)} - x^2\right) + \frac{\beta\psi - \alpha}{\beta^2}\right]^{1/2}, \tag{112}$$

where $x(s)$ solves (107) with the boundary conditions $x \to \pm\sqrt{\frac{\psi}{\alpha}}$ as $s \to \pm\infty$.

Once the heteroclinic orbit is found, we can transform the solution back to the original variables, $\boldsymbol{\kappa}$ and $\mathbf{x}$. We then have an approximation to the solution representing a perversion. In Figure 15, the curvature and twist density obtained in this manner are shown and are compared with the exact fixed points. The corresponding filaments are shown in Figure 16.

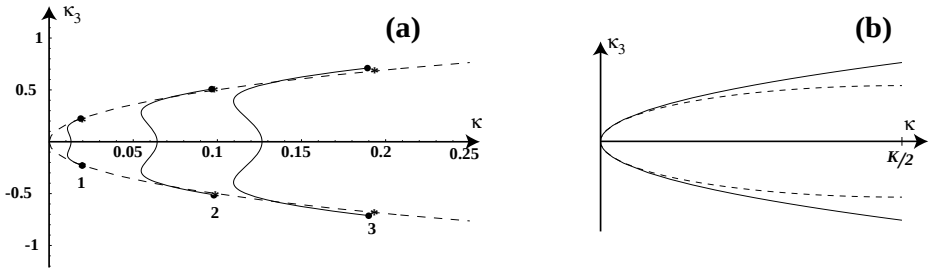

Fig. 15. Comparison of solutions on the center manifold with exact fixed points, ($\Lambda = 1, \Gamma = \frac{3}{4}, K = 2$). The dashed curve represents the part of the ellipse of fixed points. (a) The heteroclinic orbit mapped to curvature and twist density. Values of μ are $-.1$, $-.05$, and $-.01$. The stars are the exact fixed points for the given values of the parameters, for each given value of μ, of the original system representing helices. Circles are the fixed points of the center manifold equations, mapped back to the original variables. (b) The curve of fixed points from the center manifold. The solid curve consists of fixed points of the center manifold equations, mapped to the original variables.

5.2. Asymmetric Cross-Sections

In the general case, where the cross-section is not symmetric ($1 \neq \Lambda \in \mathbb{R}^+$), the reduced system (98–99) on the center manifold cannot be integrated. Nevertheless, we can further simplify it by a normal form computation [64]. We apply a near-identity transformation

$$\mathbf{W} = \mathbf{C} + \mathbf{P}(\mathbf{C}), \tag{113}$$

where $\mathbf{P}(\mathbf{C})$ is a polynomial, beginning with quadratic terms, chosen to simplify the equation for $\mathbf{C}$. In our case, since the Jacobian matrix at the bifurcation ($\psi = 0$) is not semisimple, the normal form is not unique [66]. However, we can choose $\mathbf{P}(\mathbf{C})$ in such a way as to eliminate all nonlinear terms in the first equation. Choosing

$$\mathbf{P}(\mathbf{C}) = \begin{pmatrix} 0 \\ C_2\Gamma\,(K^2(2\,\Gamma^2 - \Gamma(8+\Lambda) + 2(4 - 2\,\Lambda + \Lambda^2))\,{C_2}^2 \\ \quad -12\,\Gamma(2+\Lambda-\Gamma)(1-\Lambda)\Lambda\,{C_3}^2)/(12\,K^4\Lambda) \\ \Gamma(2\,\Gamma^2 - \Gamma(8+\Lambda) + 2(4-\Lambda^2))\,{C_2}^2\,C_3/(4\,K^2\,\Lambda) \end{pmatrix}, \tag{114}$$

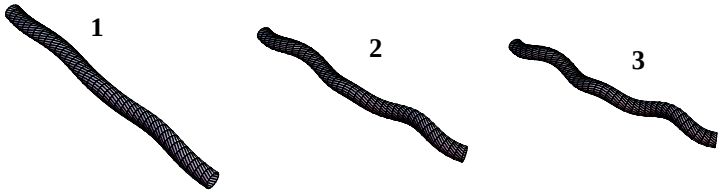

Fig. 16. The filaments corresponding to the heteroclinic orbits in Figure 15.

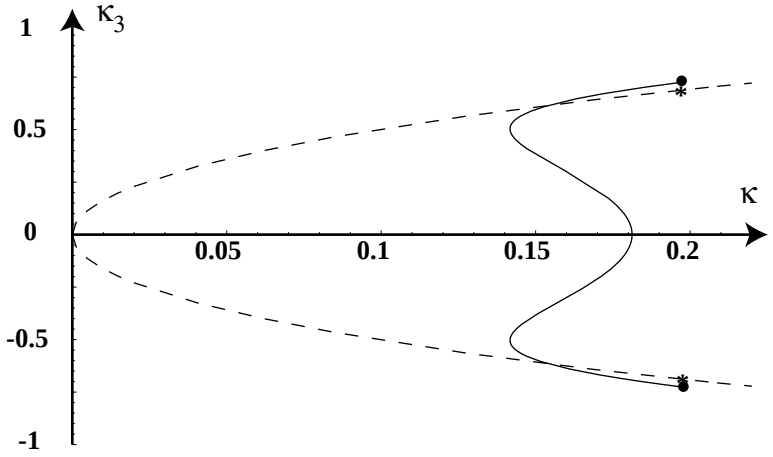

Fig. 17. A heteroclinic orbit in the asymmetric case. $\Lambda = 0.5, \Gamma = .75, K = 2, \mu = -0.1$. The dashed curve is the curve of fixed points representing helices. Stars are the exact fixed points for the given values of the parameters. Compare with Figure 15.

and dropping order four and higher terms, the equation for **C** becomes

$$x' = y, \tag{115}$$

$$y' = x(-\psi + \alpha x^2), \tag{116}$$

or, equivalently, $x'' = x(-\psi + \alpha x^2)$, where $x = C_2$, $y = C_3$, and ψ, $\alpha = \alpha_2$ are as in (102–104). There is a heteroclinic orbit connecting the two fixed points $\pm\sqrt{\psi/\alpha}$. The fixed points, as before, represent helices, and the heteroclinic orbit a perversion (see Fig. 17), given by

$$x(s) = \sqrt{\frac{\psi}{\alpha}}\,\tanh\left(s\sqrt{\frac{\psi}{2}}\right), \qquad y(s) = \frac{\psi}{\sqrt{2\alpha}}\,\mathrm{sech}^2\left(s\sqrt{\frac{\psi}{2}}\right). \tag{117}$$

An explicit approximation to the perversion solution as a function of s correct to third order can be obtained by writing this solution in terms of the original variables.

Note that there is no bifurcation of the system (115–116) at $\Lambda = 1$. The behavior of rods in this case is similar for rods with symmetric and slightly asymmetric cross-sections. This contrasts with the case studied in [49], in which a rod without intrinsic curvature is twisted at its ends. In that case, a bifurcation occurs at $\Lambda = 1$, and the behavior is markedly different in the symmetric and asymmetric cases. In the case of a rod with intrinsic curvature, the symmetry is already broken by the addition of intrinsic curvature. Thus, the addition of a nonsymmetric cross-section does not change the asymmetry of the system, and hence has no effect on the qualitative behavior of solutions.

6. The General Reduction

We can obtain a more general picture of the dynamics that includes all bounded orbits on the center manifold around $\mathbf{X}^*$ by deriving the center manifold and normal form equations of the entire system (26–31) without using the first integrals. In this setting, we can show that two families of homoclinic orbits exist. These homoclinic orbits collapse to a pair of heteroclinic orbits, the perversion solutions. In addition to yielding the perversion solution as the collapse of homoclinic orbit, we also discover families of periodic orbits. The normal form gives a picture of the full dynamics in a simplified three-dimensional system.

6.1. Reduction to the Center Manifold

We proceed as in the previous section, first reducing to a center manifold, and then deriving the normal form equations. Setting $\tilde{\mathbf{X}} = (F_1, F_2, \tilde{F}_3, \kappa_1, \kappa_2, \kappa_3, \mu)^T$, where $\tilde{F}_3 = F_3 - \phi^2$, $\mu = \phi - \phi_c$, as before, we can write the static Kirchhoff equation as the extended system

$$\tilde{\mathbf{X}}' = \mathbf{A}\tilde{\mathbf{X}} + \mathbf{h}(\tilde{\mathbf{X}}), \tag{118}$$

where the last equation reads $\mu' = 0$, and $\mathbf{h}(\tilde{\mathbf{X}})$ contains only nonlinear terms. The origin, $\tilde{\mathbf{X}} = 0$, represents the straight rod at the critical tension. Transforming the linear part into Jordan form by $\tilde{\mathbf{X}} = \mathbf{SY}$ where $\mathbf{S}^{-1}\mathbf{AS} = \mathbf{J}$ is in Jordan form, we obtain

$$\mathbf{Y}' = \mathbf{JY} + \mathbf{G}(\mathbf{Y}), \tag{119}$$

where

$$\mathbf{J} = \begin{pmatrix} 0 & 0 & 0 & 0 & 0 & 0 & 0 \\ 0 & 0 & 0 & 0 & 0 & 0 & 0 \\ 0 & 0 & 0 & 1 & 0 & 0 & 0 \\ 0 & 0 & 0 & 0 & 1 & 0 & 0 \\ 0 & 0 & 0 & 0 & 0 & 0 & 0 \\ 0 & 0 & 0 & 0 & 0 & -K/\sqrt{\Gamma} & 0 \\ 0 & 0 & 0 & 0 & 0 & 0 & K/\sqrt{\Gamma} \end{pmatrix}. \tag{120}$$

This system can be written

$$\mathbf{W}' = \mathbf{J_1}\mathbf{W} + \mathbf{G_1}(\mathbf{W}, \mathbf{Z}), \tag{121}$$

$$\mathbf{Z}' = \mathbf{J_2}\mathbf{Z} + \mathbf{G_2}(\mathbf{W}, \mathbf{Z}), \tag{122}$$

where $\mathbf{W} = (y_1, y_2, y_3, y_4, y_5)^T$ and $\mathbf{Z} = (y_6, y_7)^T$. The eigenvalues of $\mathbf{J_1}$ are all zero, while the eigenvalues of $\mathbf{J_2}$ are $\pm K/\sqrt{\Gamma}$. The analytic center manifold tangent to the center subspace $\mathbf{Z} = \mathbf{0}$ is $\mathbf{Z} = \mathbf{H}(\mathbf{W}) = \mathbf{H}^{(2)}(\mathbf{W}) + \mathbf{H}^{(3)}(\mathbf{W}) + \cdots, \mathbf{H}^{(k)}(\mathbf{W})$ being a homogeneous polynomial of degree k in $\mathbf{W}$. As before, we solve for $\mathbf{H}^{(2)}(\mathbf{W})$,

$$\mathbf{H}^{(2)}(\mathbf{W}) = \begin{pmatrix} \frac{\Gamma(K^4 y_2{}^2 + (6-3\Gamma+4\Lambda)(\Gamma^2 y_4{}^2 - K\Gamma^{\frac{3}{2}} y_3 y_4) + K^2\Gamma((2-\Gamma+\Lambda)(y_3{}^2 + y_2 y_4 - K\Gamma^{-\frac{1}{2}} y_2 y_3) + \Lambda y_2 y_4))}{2K^5} \\ \frac{\Gamma(K^4 y_2{}^2 + (6-3\Gamma+4\Lambda)(\Gamma^2 y_4{}^2 + K\Gamma^{\frac{3}{2}} y_3 y_4) + K^2\Gamma((2-\Gamma+\Lambda)(y_3{}^2 + y_2 y_4 + K\Gamma^{-\frac{1}{2}} y_2 y_3) + \Lambda y_2 y_4))}{2K^5} \end{pmatrix}, \tag{123}$$

and the center manifold equations are

$$\mathbf{W} = \mathbf{J_1}\mathbf{W} + \mathbf{f}(\mathbf{W}) + \mathrm{O}(|\mathbf{W}|^4), \tag{124}$$

where $\mathbf{f}(\mathbf{W}) = \mathbf{G_1}(\mathbf{W}, \mathbf{H}^{(2)}(\mathbf{W}))$. We examine solutions near $\mathbf{Y} = \mathbf{0}$. We drop the order four and higher terms, and examine the resulting equation.

6.2. Normal Form Derivation and Analysis

As before, we make the near-identify transformation $\mathbf{W} = \mathbf{C} + \mathbf{P}(\mathbf{C})$. Choosing

$$\mathbf{P}(\mathbf{C}) = \begin{pmatrix} 0 \\ \frac{\Gamma}{18K^6\Lambda}(C_2(2K^4(2\Gamma^2 - \Gamma(8+3\Lambda) + 2(4+\Lambda+\Lambda^2))C_2{}^2 + 3K^2\Gamma(24+15\Gamma^2 \\ \quad + 28\Lambda - 2\Lambda^2 - \Gamma(42+26\Lambda-3\Lambda^2))C_2C_4 - 3\Gamma(K^2(6+6\Gamma^2+22\Lambda \\ \quad - 2\Lambda^2 - 6\Lambda^3 - \Gamma(15+17\Lambda-6\Lambda^2))C_3{}^2 + 6\Gamma(6-3\Gamma \\ \quad + 4\Lambda)(1-\Lambda)\Lambda C_4{}^2))) \\ -\frac{\Gamma}{6K^4\Lambda}(C_3(2K^2(-8-2\Gamma^2-5\Lambda+\Lambda^2+\Gamma(8+3\Lambda))C_2{}^2 + \Gamma(6+6\Gamma^2 \\ \quad + 10\Lambda + 4\Lambda^2 - \Gamma(15+11\Lambda))C_3{}^2 + 6(1-\Gamma)\,\Gamma(-6+3\Gamma-4\Lambda)C_2C_4)) \\ \frac{1}{6K^4\Lambda}(6K^4(-1+\Gamma)C_2{}^3 + 2K^2\Gamma(10+\Gamma^2+7\Lambda-2\Lambda^2-\Gamma(7+3\Lambda))C_2C_3{}^2 \\ \quad - 2K^2\Gamma(\Lambda+\Lambda^2-2-\Gamma(1+3\Lambda-\Gamma))C_2{}^2C_4 + 3\Gamma^2(6-3\Gamma \\ \quad + 4\Lambda)(1-\Lambda)C_3{}^2C_4) \\ \frac{\Gamma}{2K^2}C_2\,(-2\,\Gamma\,\Lambda\,C_4 + C_2\,(-K^2 + 2\,K\,\sqrt{\Gamma}\,C_1 + \Gamma\,C_5)) \end{pmatrix}, \tag{125}$$

the equation for $\mathbf{C}$ becomes

$$C_2' = C_3, \tag{126}$$

$$C_3' = C_4, \tag{127}$$

$$C_4' = C_3(\psi + \alpha C_2^2 - \beta C_3^2), \tag{128}$$

$$C_1' = C_5' = 0, \tag{129}$$

where terms of order four and higher have been neglected. C_1 is μ, and since C_5 is constant it is treated as a parameter. The normal form (126–129) is then a third-order system. The constants α and β are positive, O(1) functions of the parameters. The constant ψ is a function of the parameters and the bifurcation parameter μ:

$$\alpha = \frac{3}{2\,\Lambda}\,(4-3\Gamma)\,, \tag{130}$$

$$\beta = \frac{\Gamma}{3K^2}\left(\Gamma^2 - 2\Gamma(2+3\Lambda) + \Lambda^2 + 10\Lambda + 4\right), \tag{131}$$

$$\psi = \frac{2\mu K + \mu\sqrt{\Gamma} + c_5\sqrt{\Gamma}}{\sqrt{\Gamma}\,\Lambda} = \frac{\phi^2 - \phi_c^2 + c_5}{\Lambda}. \tag{132}$$

The following rescalings

$$C_2 = \frac{1}{\sqrt{\beta}}x, \qquad C_3 = \frac{\sqrt{\alpha}}{\beta}y, \qquad C_4 = \frac{\alpha}{\beta^{3/2}}z, \tag{133}$$

$$s = \sqrt{\frac{\beta}{\alpha}}t, \qquad \psi = \frac{\alpha}{\beta}\tilde{\psi}, \tag{134}$$

transform (126–129) into

$$x' = y, \tag{135}$$

$$y' = z, \tag{136}$$

$$z' = y(\tilde{\psi} + x^2 - y^2), \tag{137}$$

or, equivalently,

$$x''' = (x')^2(\tilde{\psi} + x^2 - (x')^2). \tag{138}$$

This normal form associated with a triple zero Jordan block is a particular case of the ζ^3 normal form defined in [66].

6.3. Normal Form Analysis

The system (135–137) has some remarkable properties which allow for a complete description of the orbits. Indeed, there exists a pair of first integrals (m_1, m_2) for this system given by

$$\begin{pmatrix} m_1 \\ m_2 \end{pmatrix} = \begin{pmatrix} \cos(\sqrt{2}x) & -\sin(\sqrt{2}x) \\ \sin(\sqrt{2}x) & \cos(\sqrt{2}x) \end{pmatrix} \begin{pmatrix} y^2 - x^2 + 1 - \tilde{\psi} \\ \sqrt{2}(z - x) \end{pmatrix}. \tag{139}$$

These two first integrals can be used to integrate explicitly the equation of motion. Let $\Theta(x) = \psi - 1 + m_1 \cos(\sqrt{2}x) + m_2 \sin(\sqrt{2}x)$, then

$$y = \pm\sqrt{x^2 + \Theta(x)}, \tag{140}$$

$$z = \frac{1}{2}\Theta'(x) + x, \tag{141}$$

where $x(t)$ solves $x' = \pm\sqrt{x^2 + \Theta(x)}$. In order to understand the geometry of the solutions, we note that the x-axis is a line of fixed points, and we consider the polynomial first integral

$$\begin{aligned} I &= m_1^2 + m_2^2 - (1 - \tilde{\psi})^2, \\ &= -4xz + y^4 + 2z^2 + y^2[2(1 - \tilde{\psi}) - 2x^2] + x^2(2\tilde{\psi} + x^2), \end{aligned} \tag{142}$$

and the surfaces $S_C = \{(x, y, z) \in \mathbb{R}^3 | I = C\}$. For fixed values of $\tilde{\psi}$, we can describe the dynamics on the surface S_C for increasing values of C.

- For $C < -\tilde{\psi}^2$, S_C has no intersection with the x-axis and there is no localized solution.
- For $-\tilde{\psi}^2 < C < 0$, there are four fixed points on S_C and there is a pair of homoclinic orbits surrounding an open set of periodic orbits.

- For $C = 0$, two of the fixed points coalesce, and again there is a pair of homoclinic orbits and two families of periodic orbits.
- For $0 < C < \tilde{C}$, there are two homoclinic orbits to the two fixed points on S_C and an open set of periodic orbits.
- For $C = \tilde{C}$, the two homoclinic orbits collapse to a pair of heteroclinic orbits and there is no periodic orbit on $S_{\tilde{C}}$. The value $\tilde{C}$ is obtained by using the parameterization of the orbits in terms of m_1, m_2 and is found to be

$$\tilde{C} = \frac{2x_1^2}{\sin\sqrt{2}x_1} - (1 - \tilde{\psi})^2, \tag{143}$$

where x_1 is the intersection point of $S_{\tilde{C}}$ with the x-axis, that is

$$x_1^2 + \tilde{\psi} - 1 + \sqrt{2}x_1 \cot(\sqrt{2}x_1) = 0. \tag{144}$$

Normal form dynamics are seen in Figure 18. The pair of homoclinic orbits for $\mu = -.1$ is seen in Figure 19. These orbits connect helices with the same handedness, the total twist does not vanish, and these are not perversions. The family of heteroclinic orbits is seen in Figures 21 and 22.

7. Numerics

The major limitation of the method we have described for computing the heteroclinic orbits representing perversions is that the normal form approximation is only valid in a neighborhood of the point $X^* = (0, 0, \phi^2, 0, 0, 0)$. As one can observe in Figure 15, the approximation loses its validity as κ and τ increase, or equivalently, as the applied tension decreases. In this section, we compare the approximate solutions with solutions computed numerically. The strategy we use in computing the orbits is to first find an orbit using a shooting method, and then to find the remaining orbits by continuation, using the software package AUTO. In computing the first orbit by shooting, we place one initial point on the unstable manifold of one fixed point and compute forward, and another initial point on the stable manifold of the other fixed point and compute backward. Then we adjust the initial points until the two orbits match. We are looking for the heteroclinic connection between the fixed points

$$\mathbf{X}_\pm(\kappa) = (\pm\gamma\kappa\tau, 0, \gamma\tau^2, \kappa, 0, \pm\tau). \tag{145}$$

The linear eigenvalues of these fixed points are $0, \pm\sigma \pm i\nu$. Therefore, the stable and unstable manifolds have dimension 2, and the tangent subspaces are spanned by the stable and unstable eigenvectors $\mathbf{v}_\pm^{(s)}$, $\mathbf{v}_\pm^{(u)}$ and their complex conjugates. Here, $\mathbf{v}_\pm$ denotes an eigenvector of the Jacobian at the fixed point $\mathbf{X}_\pm$. Thus, we compute two initial value problems, placing our initial conditions at

$$\mathbf{X}(0) = \mathbf{X}_+ + \epsilon[\mathrm{Re}(\mathbf{v}_+^{(u)})\cos(\theta_+) + \mathrm{Im}(\mathbf{v}_+^{(u)})\sin(\theta_+)], \tag{146}$$

$$\mathbf{X}(0) = \mathbf{X}_- + \epsilon[\mathrm{Re}(\mathbf{v}_-^{(s)})\cos(\theta_-) + \mathrm{Im}(\mathbf{v}_-^{(s)})\sin(\theta_-)], \tag{147}$$

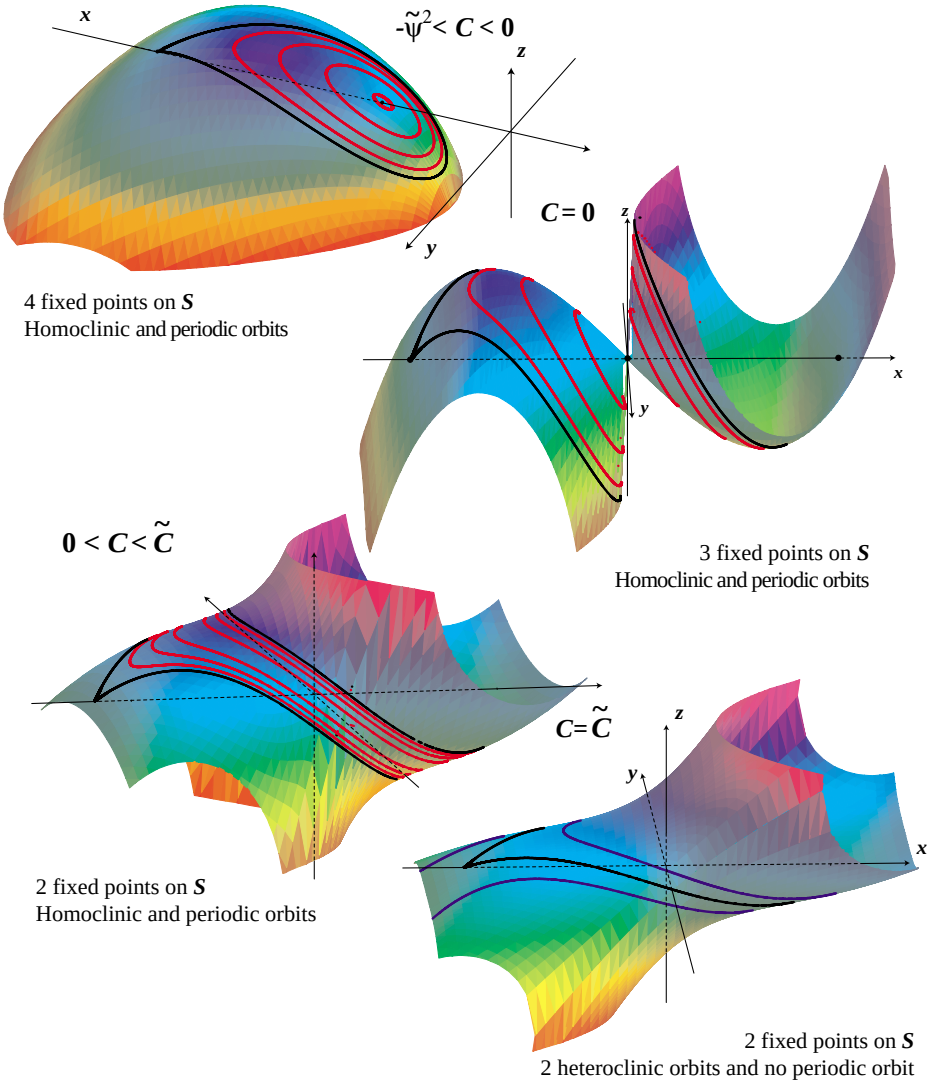

Fig. 18. Normal form dynamics for various values of C.

and computing forward and backward, respectively, at time T. The value of ϵ is taken to be very small, typically 10^{-5}, so that the initial conditions lie close to the unstable and stable manifolds. There is no family of heteroclinic orbits connecting each pair of fixed points. Rather, there is a unique pair of values of $\theta_{\pm}$ such that the orbits connect. The angles $\theta_{\pm}$ and T are then adjusted until the two orbits coincide. The three first integrals I_1, I_2, I_3 are used as diagnostics to check the accuracy of the numerical solutions. The results of one computation are seen in Figure 20.

Once we have computed one heteroclinic orbit, we use this as a starting point to compute by continuation the remaining orbits. We use the HomCont routines in the

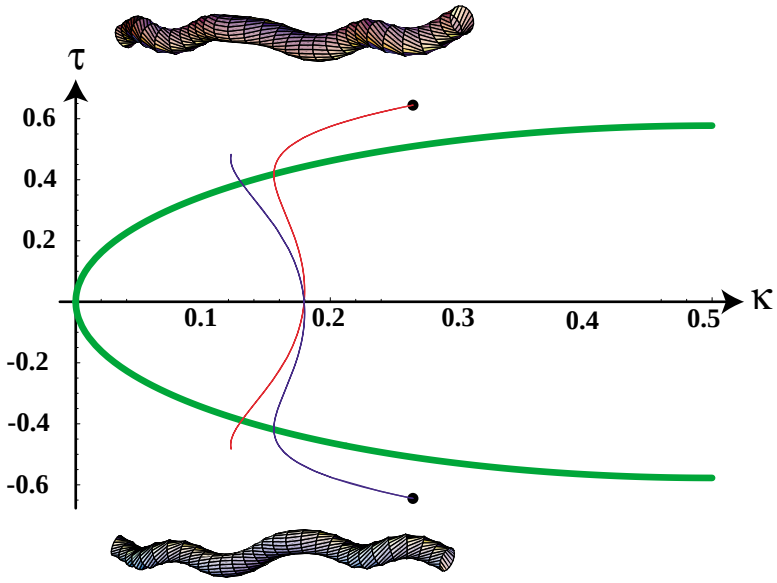

Fig. 19. A pair of homoclinic orbits from the normal form in the curvature-torsion plane together with the corresponding filaments. Note that these orbits connect helices with the same handedness.

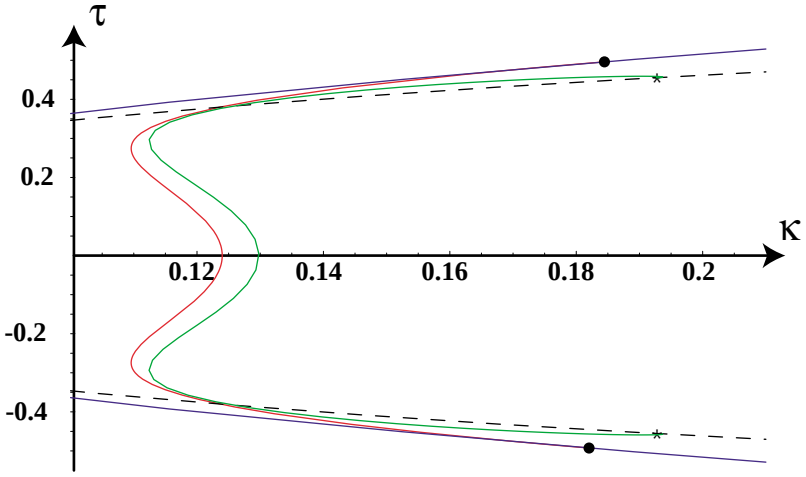

Fig. 20. Comparison of numerical and normal form solutions. Shown are a numerical solution connecting the actual fixed points labeled by *'s, and the normal form approximation connecting the approximate fixed points labeled by a black dot. Values of the parameters are $K = 1$, $\Lambda = 1$, $\Gamma = 0.75$, $\mu = -0.1$.

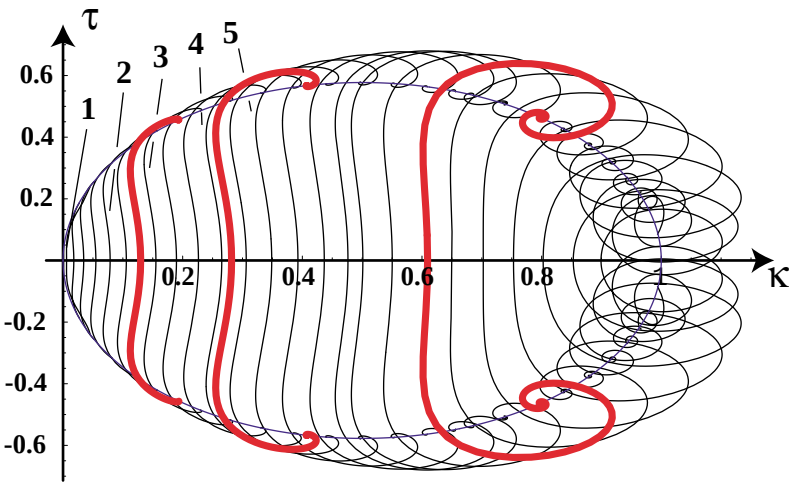

Fig. 21. Family of heteroclinic orbits. Projections in the $\kappa - \tau$ plane. The thick curves represent orbits computed by shooting, the thin curves are those computed by continuation. Values of the parameters are $K = 1$, $\Lambda = 1$, $\Gamma = 0.75$.

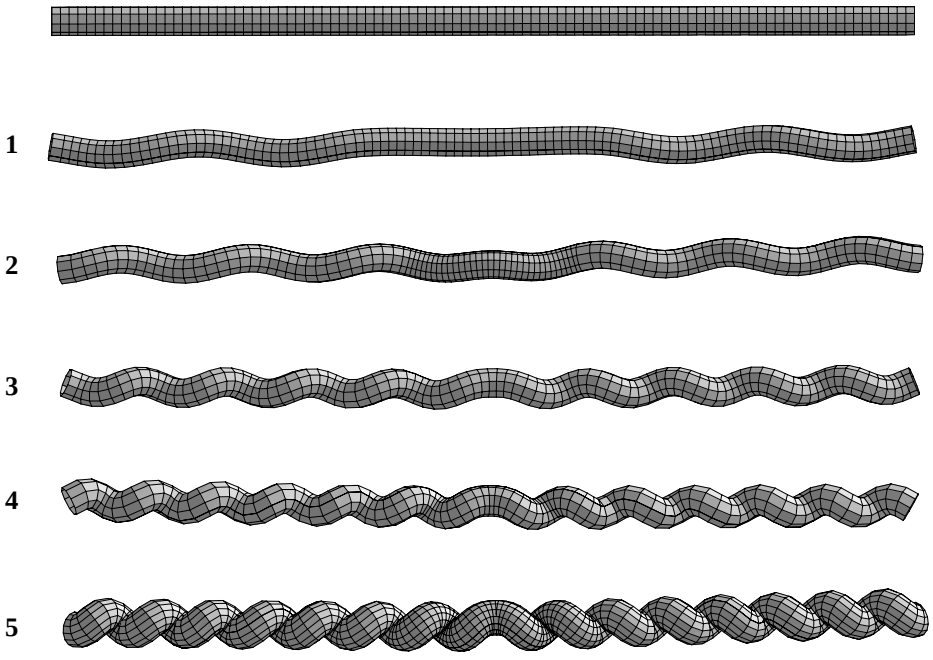

Fig. 22. Family of heteroclinic orbits. Perversions for varying values of tension. Values of the parameters are $K = 1$, $\Lambda = 1$, $\Gamma = 0.75$.

AUTO 97 package [67] to continue these orbits, and compute the family of heteroclinic orbits connecting the points $\mathbf{X}_{\pm}(\kappa)$ for $0 < \kappa < K$. Figure 22(a) shows the family of orbits computed in this manner, projected onto the $\kappa - \tau$ plane. Figure 22(b) shows a family of perversion solutions.

8. Conclusions

In the world of elastic filaments there are two fundamental instabilities responsible for producing complex three-dimensional structures. The first one is the well-known coiling instability. It transforms local twist into writhe and produces a large coiled structure whose handedness is inherited from the handedness of the twist. In this paper, we studied the second type of instability whereby a change in the curvature deficit (the difference between local and intrinsic curvatures) produces a global change of the structure by creating structures with no preferred handedness. In the context of the Kirchhoff equations for elastic rods, perversion is modeled as a heteroclinic orbit connecting two fixed points representing asymptotic helices. We found the relationship between the tension applied at the ends of the filament and the curvature of these helices. We identified both the critical value of the tension below which a straight rod with intrinsic curvature becomes unstable and is replaced by a perversion and the specific value of the applied tension such that the asymptotic helices are in self-contact. Therefore, we computed the upper and lower value of the applied tension for which a perversion can exist. Since the effect of the intrinsic curvature is to break the symmetry of the elastic properties of the cross-sections, a geometric asymmetry in the cross-section plays no role in the qualitative picture given here. Likewise the presence of a small intrinsic twist does not modify the overall qualitative picture given here. An intriguing problem arises when both intrinsic curvature and intrinsic twist are sufficiently large as to create an instability. We expect that there should be a subtle interplay between the two types of bifurcations around these values.

The new structure formed through this instability and composed of two helices connected by an inversion is a twistless spring. We computed the characteristic of this spring and showed how it deviates from Hooke's law. The functional advantage for a tendril or any similar structure to form a perversion appears clearly. A relatively fragile filament can form a perversion and create a spring that can withstand much heavier loads before breaking. This observation was first made by Darwin [14], to whom we leave the last word: "I have more than once gone on purpose during a gale to watch a Bryony growing in an exposed hedge, with its tendrils attached to the surrounding bushes; and as the thick and thin branches were tossed to and fro by the wind, the tendrils, had they not been excessively elastic, would instantly have been torn off and the plant thrown prostrate. But as it was, the Bryony safely rode out the gale, like a ship with two anchors down, and with a long range of cable ahead to serve as a spring as she surges to the storm."

Appendix A: Helical Filaments Are Twistless

Proposition A.1. *Consider the static Kirchhoff equation (17–19) with intrinsic curvature* $\boldsymbol{\kappa}^{(u)} = K\,\mathbf{d}_1 + \tau_0\,\mathbf{d}_3$. *Then (i) the only solutions with constant curvature and torsion*

are twistless helices (i.e., $\zeta' = 0$); (ii) constant solutions are either twistless helices or twisted straight rods.

In other words, the set of fixed points of (17–19) with $\boldsymbol{\kappa}^{(u)} = K\,\mathbf{d}_1 + \tau_0\,\mathbf{d}_3$ is exactly the set of twistless helices and twisted straight rods.

Proof. Suppose, first, that the cross-section of the filament is symmetric, so that $\Lambda = 1$. Substituting $\boldsymbol{\kappa} = (\kappa\sin(\zeta), \kappa\cos(\zeta), \tau + \zeta')$, $\boldsymbol{\kappa}^{(u)} = K\,\mathbf{d}_1 + \tau_0\,\mathbf{d}_3$, where κ, K, τ, and τ_0 are constant, into the original static equations (17–19), we have the system

$$F_1{}' = -\kappa\,\cos(\zeta)\,F_3 + F_2(\tau + \zeta'), \tag{148}$$

$$F_2{}' = \kappa\,\sin(\zeta)\,F_3 - F_1(\tau + \zeta'), \tag{149}$$

$$F_3{}' = \kappa(\cos(\zeta)\,F_1 - \sin(\zeta)\,F_2), \tag{150}$$

$$\kappa\,\cos(\zeta)\,\zeta' = F_2 + \kappa\,\cos(\zeta)(\Gamma\tau_0 + (1-\Gamma)(\tau + \zeta')), \tag{151}$$

$$-\kappa\,\sin(\zeta)\,\zeta' = -F_1 - \kappa\,\Gamma\,\tau_0\,\sin(\zeta) + (K - \kappa(1-\Gamma)\,\sin(\zeta))(\tau + \zeta'), \tag{152}$$

$$\zeta'' = -\frac{\kappa\,K}{\Gamma}\cos(\zeta). \tag{153}$$

Solving (148–153) for F_1 and F_2, we obtain

$$F_1(s) = \tau\,K + K\,\zeta' + [\tau\,\kappa\,(\Gamma - 1) + \kappa\,\Gamma\,(\zeta' - \tau_0)]\sin(\zeta), \tag{154}$$

$$F_2(s) = \kappa[\tau(\Gamma - 1) - \Gamma\,(\tau_0 - \zeta')]\cos(\zeta). \tag{155}$$

Differentiating (154), equating the result with (148), and using (153), we obtain

$$\cos(\zeta)[K^2 - \Gamma\,\tau^2 + \Gamma^2\,\tau^2 + \kappa\,K\,\Gamma\,\sin(\zeta) - \Gamma\,F_3(s) + \Gamma^2\,\tau\tau_0 + \Gamma^2\,\tau\,\zeta'] = 0. \tag{156}$$

Either $\cos(\zeta) = 0$ or the other factor of the LHS of the previous equation is zero. Differentiating this factor with respect to s, and using (153, 154, 155) again, we obtain

$$\cos(\zeta) = 0. \tag{157}$$

This implies that, since $\kappa \geq 0$, $\sin(\zeta) = 1$. Using this result in (148–153), we can solve for $\mathbf{F}$ and $\boldsymbol{\kappa}$, to obtain

$$\boldsymbol{\kappa} = \kappa\mathbf{d}_1 + \tau\mathbf{d}_3, \tag{158}$$

$$\mathbf{F} = \gamma\tau\boldsymbol{\kappa}, \tag{159}$$

where

$$\gamma = \left(\frac{K}{\kappa} - 1 + \Gamma\left(1 - \frac{\tau_0}{\tau}\right)\right). \tag{160}$$

In the asymmetric case ($\Lambda \neq 1$), substituting $\boldsymbol{\kappa} = (\kappa\sin(\zeta), \kappa\cos(\zeta), \tau + \zeta')$, $\boldsymbol{\kappa}^{(u)} = K\,\mathbf{d}_1 + \tau_0\,\mathbf{d}_3$, where κ, K, τ, and τ_0 are constant, into the original static equations (17–19), we solve, as before, for F_1 and F_2 in terms of ζ. Substitution into (17) provides us with the following equation:

$$\cos(\zeta)A(\zeta, \zeta', F_3) = 0, \tag{161}$$

where the form of A is omitted. As before, we proceed by eliminating all possibilities but $\cos(\zeta) = 0$. If $\cos(\zeta) \neq 0$, then we differentiate the second factor in the previous equation. This gives us an equation in ζ, ζ' and $\sin(\zeta)$. We then solve for ζ' and subtract the result of solving for ζ' in the sixth equation of (17–19). We thus arrive at an equation of the form

$$\sum_{n=0}^{4} a_n \sin^n(\zeta) = 0, \tag{162}$$

where the a_n's are constants in s. A contradiction is then reached if ζ is not constant, since not all of the coefficients a_n are zero. It must be, then, that $\zeta' = 0$, and substituting this result into (148–153), we get (158–159) again.

For the second part of the statement, we note that if $\boldsymbol{\kappa}' = 0$, then

$$\frac{d}{ds}\frac{1}{2}\kappa^2 = \frac{d}{ds}\frac{1}{2}(\kappa_1^2 + \kappa_2^2) = \kappa_1\kappa_1' + \kappa_2\kappa_2' = 0, \tag{163}$$

so that curvature is constant. We thus have

$$\kappa_1' = \kappa\cos(\zeta)\zeta' = 0 = -\kappa\sin(\zeta)\zeta' = \kappa_2'. \tag{164}$$

This implies that either $\kappa = 0$ (zero curvature—a straight rod) or $\zeta' = 0$ (zero twist). In the case $\zeta' = 0$,

$$\kappa_3' = \tau' = 0, \tag{165}$$

so that torsion is constant. In this case the rod is a twistless helix. In the case of zero curvature the rod may be twisted. □

Acknowledgments

The authors would like to thank Michael Tabor and Ray Goldstein for many fruitful discussions, and Eusebius Doedel, Bjorn Sandstede, and Alan Champneys for invaluable help in computing the continuation solutions. T. M. is supported through the NSF-VIGRE initiative. A. G. is a Sloan fellow. This work is supported by the NSF grant DMS-9972063 (A. G.).

References

[1] F. H. C. Crick. Linking numbers and nucleosomes. *Proc. Natl. Acad. Sci. USA*, 73:2639–2643, 1976.

[2] F. B. Fuller. Decomposition of the linking number of a closed ribbon: A problem from molecular biology. *Proc. Natl. Acad. Sci. USA*, 78:3557–3561, 1978.

[3] C. J. Benham. Geometry and mechanics of DNA superhelicity. *Biopolymers*, 22:2477–2495, 1983.

[4] N. H. Mendelson. Helical *bacillus subtilis* macrofibers: Morphogenesis of a bacterial multicellular macroorganism. *Proc. Natl. Acad. Sci. USA*, 75:2472–2482, 1978.

[5] N. H. Mendelson. Bacterial macrofibers: The morphogenesis of complex multicellular bacterial forms. *Sci. Prog. Oxford*, 74:425–441, 1990.
[6] I. Klapper and M. Tabor. Dynamics of twist and writhe and the modeling of bacterial fibers. In J. Mesirov, K. Schuiten, and De Witt Summers, editors, *Mathematical Approaches to Biomolecular Structure and Dynamics*, pages 139–159. Springer-Verlag, New York, 1996.
[7] A. Goriely and M. Tabor. Spontaneous helix-hand reversal and tendril perversion in climbing plants. *Phys. Rev. Lett.*, 80:1564–1567, 1998.
[8] J. B. Listing. Vorstudien über topologie. *Göttinger Studien*, I:811–875, 1847.
[9] N. Biggs, E. K. Lloyd, and R. J. Wilson. *Graph theory*. Clarendon, Oxford, 1976.
[10] D'Arcy W. Thomspon. *On growth and form: The complete revised edition*. Dover, New York, 1992.
[11] J. C. Maxwell. *A treatise on electricity and magnetism*. Clarendon, Oxford, 1873.
[12] S. J. Gould. Covariance sets and ordered geographic variation in *cerion* from Aruba, Bonaire, and Curaçao: A way of studying nonadaptation. *Systematic Zoology*, 33:217–237, 1984.
[13] R. Robertson. Snail handedness. *Natl. Geogr. Res. Explor.*, 9:120–131, 1993.
[14] Ch. Darwin. *The movements and habits of climbing plants*. Appleton, New York, 1888. Darwin's book is available online at the Project Gutenberg: `http://promo.net/pg/`.
[15] K. Larson. Circumnutation behavior of an exotic honeysuckle vine and its native congener: Influence on clonal mobility. *Am. J. Bot.*, 87:533–538, 2000.
[16] S. Lubkin. Unidirectional waves on rings: Models for chiral preferences of circumnutating plants. *Bull. Math. Biol.*, 56:795–810, 1994.
[17] C. Linnaei. *Philosophia Botanica*. Stockholm, 1751.
[18] A. P. de Candolle. *Organographie végétale*. Chez Deterville, Paris, 1827.
[19] A. P. de Candolle. *Physiologie végétale*. Béchet Jeune, Paris, 1832.
[20] M. Dutrochet. Recherche sur la volubilité des tiges de certains végétaux et sur la cause de ce phé nomène. *C. R. Acad. Sci.*, 19:295–303, 1844.
[21] H. von Mohl. *Principles of the anatomy and physiology of the vegetable cell*. John van Voorst, Paternoster Row, London, 1852.
[22] I. Léon. Recherche nouvelles sur la cause du mouvement spiral des tiges volubiles. *Bull. Soc. Bot. France*, 5:351–356, 1858.
[23] I. Léon. Recherche nouvelles sur la cause du mouvement spiral des tiges volubiles (deuxième partie). *Bull. Soc. Bot. France*, 5:610–685, 1858.
[24] A. Gray. Note on the coiling of tendrils. *Proc. Am. Acad. Arts & Sci.*, 4:98–100, 1858.
[25] P. Malpas and A. M. Symonds. Observations on the structure of the human umbilical cord. *Surg. Gynecol. Obstet.*, 123:746–750, 1966.
[26] H. W. Edmonds. The spiral twist of the normal umbilical cord in twins and singletons. *Am. J. Obstet. & Gynecol.*, 67:102–120, 1954.
[27] B. D. Chaurasia and B. M. Agarwal. Helical structure of the human umbilical cord. *Acta Anat.*, 103:226–230, 1979.
[28] G. Ente and P. H. Penzer. The umbilical cord: Normal parameters. *J. Roy. Soc. Health*, August:138–140, 1991.
[29] R. V. Lacro, K. L. Jones, and K. Benirschke. The umbilical cord twist: Origin, direction, and relevance. *Am. J. Obstet. Gynecol.*, 157:833–838, 1987.
[30] W. Blackburn, N. R. Cooley, and E. A. Manci. Correlations between umbilical cord structure—composition and normal and abnormal fetal devlopment. In R. A. Saul, editor, *Proceedings of the Greenwood Genetics Conference*, pages 180–181. Jacobs Press, Clinton, S.C., 1988.
[31] A. C. Moessinger, W. A. Blanc, P. A. Marone, and D. C. Polsen. Umbilical cord length as an index of fetal activity: Experimental study and clinical implications. *Pediatr. Res.*, 16:109–112, 1982.

[32] S. Barron, J. A. Foss, and E. P. Riley. The effect of prenatal cocaine exposure on umbilical cord length in fetal rats. *Neurotoxicol. Teratol.*, 13:503–506, 1991.
[33] R. M. Macnab and M. K. Ornston. Normal-to-curly flagellar transitions and their role in bacterial tumbling. Stabilization of an alternative quaternary structure by mechanical force. *J. Mol. Biol.*, 112:1–30, 1977.
[34] C. R. Calladine. Change of waveform in bacterial flagella: The role of mechanics at the molecular level. *J. Mol. Biol.*, 118:457–479, 1978.
[35] D. L. D. Caspar. Bacterial flagellar coiling explained by slip-and-click strand switching. *Nat. Struct. Biol.*, 5:92–94, 1998.
[36] I. Yamashita, K. Hasegawa, H. Suzuki, F. Vonderiszt, Y. Mimori-Kiyosue, and K. Namba. Structure and switching of bacterial flagellar filaments studied by X-ray diffraction. *Nat. Struct. Biol.*, 5:125–132, 1998.
[37] H. C. Berg and R. A. Anderson. Bacteria swin by rotating their flagellar filaments. *Nature*, 245:380–383, 1973.
[38] R. Kamiya, S. Asakura, K. Wakabayashi, and K. Namba. Transition of bacterial flagella from helical to straight forms with different subunits arrangements. *J. Mol. Biol.*, 131:725–754, 1979.
[39] L. Turner, W. S. Ryu, and H. C. Berg. Real-time imaging of fluorescent flagellar filaments. *J. Bacteriol.*, 182:2793–2801, 2000.
[40] R. Goldstein, A. Goriely, G. Hubber, and C. Wolgemuth. Bistable helices. *Phys. Rev. Lett.*, 84:1631–1634, 2000.
[41] S. F. Goldstein and N. W. Charon. Motility of the spirochete *Leptospira*. *Cell Motility Cytoskeleton*, 9:101–110, 1988.
[42] M. J. Tilby. Helical shape and wall synthesis in a bacterium. *Nature*, 266:450–552, 1977.
[43] L. Waterkeyn. Light microscopy of the cotton fibre. In *Cotton fibres: Their development and properties*. International Institute for Cotton, Manchester, U.K., 1985.
[44] J. J. Vermeulen. Notes on the non-marine molluscs of the island of Borneo: The genus Opisthostoma (Gastropoda Prosobranchia; Diplommatinidae), part 2. *Basteria*, 58:73–191, 1994.
[45] J. W. S. Hearle, J. J. Thwaites, and J. Amirbayat (eds.). *Mechanics of flexible fibre assemblies*. Sijthoff & Noordhoff, The Netherlands, 1980.
[46] J. B. Keller. Tendril shape and lichen growth. *Lect. Math. Life Sci.*, 30:257–274, 1980.
[47] P. Mielke and A. Holmes. Spatially complex equilibria of buckled rods. *Arch. Ratl. Mech. Anal.*, 101:319–348, 1988.
[48] A. R. Champneys and J. M. T. Thompson. A multiplicity of localized buckling modes for twisted rod equations. *Proc. Roy. Soc. Lond. A*, 452:2467–2491, 1996.
[49] G. H. M. van der Heijden, A. R. Champneys, and J. M. T. Thompson. The spatial complexity of localized buckling in rods with non-circular cross-section. *SIAM J. Appl. Math.*, 59:198–221, 1998.
[50] R. S. Manning and K. A. Hoffman. Stability of n-covered circles for elastic rods with constant planar intrinsic curvature. *J. Elast.*, 62:23–46, 2001.
[51] P. Shipman and A. Goriely. On the dynamics of helical strips. *Phys. Rev. E*, 61:4508–4517, 2000.
[52] A. R. Champneys, G. H. M. van der Heijden, and J. M. T. Thompson. Spatially complex localization after one-twist-per-wave equilibria in twisted circular rods with initial curvature. *Phil. Trans. Roy. Soc. Lond. A*, 355:2151–2174, 1997.
[53] H. J. Zhou and Z. C. Ou-Yang. Spontaneous curvature-induced dynamical instability of Kirchhoff filaments: Application to DNA kink deformations. *J. Chem. Phys.*, 110:1247–1251, 1999.
[54] S. S. Antman. *Nonlinear problems of elasticity*. Springer-Verlag, New York, 1995.

[55] B. D. Coleman, E. H. Dill, M. Lembo, Z. Lu, and I. Tobias. On the dynamics of rods in the theory of Kirchhoff and Clebsch. *Arch. Ratl. Mech. Anal.*, 121:339–359, 1993.
[56] A. Goriely, M. Nizette, and M. Tabor. On the dynamics of elastic strips. *J. Nonlinear Sci.* 11:3–45:2001.
[57] W. K. Silk. On the curving and twining of stems. *Environmental Exp. Bot.*, 29:95–109, 1989.
[58] J. J. Mertens. The shape and stabilization of the crimp in false-twist thermoplastic yarn. In *Bulk, stretch and texture: Papers of the 61st annual conference of the Textile Institute*, 42–53, 1966.
[59] W. K. Silk. Growth rate patterns which maintain a helical tissue tube. *J. Theor. Biol.*, 138:311–327, 1989.
[60] J. Marsden and T. Ratiu. *Classical mechanics*. Springer-Verlag, New York, 1994.
[61] A. Goriely. *Integrability and nonintegrability in dynamical systems*. World Scientific, Singapore, 2001.
[62] S. Przybyl and P. Pieranski. Helical close packing. *Eur. Phys. J. E*, 4:445–449 2001.
[63] A. Maritan, C. Micheletti, A. Trovato, and J. R. Banavar. Optimal shapes of compact strings. *Nature*, 406:287–290, 2000.
[64] J. Guckenheimer and P. Holmes. *Nonlinear oscillations, dynamical systems and bifurcations of vector fields*. Springer-Verlag, New York, 1983.
[65] S. Wiggins. *Global bifurcations and chaos*. Springer-Verlag, New York, Berlin, 1988.
[66] C. Elphick, E. Tirapegui, M. E. Brachet, P. Coullet, and G. Iooss. A simple global characterization for normal forms of singular vector fields. *Physica D*, 29:95–127, 1987.
[67] E. J. Doedel, A. R. Champneys, T. R. Fairgrieve, T. R. Kuznetsov, A. Yu, B. Sandstede, and X. J. Wang. AUTO97 continuation and bifurcation software for ordinary differential equations. Available by anonymous ftp from `FTP.CS.CONCORDIA.CA` directory `PUB/DOEDEL/AUTO`.